NASA Technical Memorandum 104792

67P

Analysis of the Shuttle Orbiter Reinforced Carbon-Carbon Oxidation Protection System

S. D. Williams
Donald M. Curry
Dennis Chao
Vuong T. Pham

June 1994

NASA Technical Memorandum 104792

Analysis of the Shuttle Orbiter Reinforced Carbon-Carbon Oxidation Protection System

S. D. Williams
Lockheed Engineering Sciences Company

Donald M. Curry
Vuong T. Pham
Lyndon B. Johnson Space Center
Houston, Texas

Dennis Chao
Rockwell International

National Aeronautics and
Space Administration

Preface

This technical memorandum is an expanded version of AIAA 94-2084, Ablation Analysis of the Shuttle Orbiter Oxidation-Protected Reinforced Carbon-Carbon (RCC), presented at the sixth AIAA/ASME Joint Thermophysics and Heat Transfer Conference, June 20-23, 1994, Colorado Springs, Colorado. This memorandum contains additional figures, discussion, and appendices which could not be included in the AIAA paper due to page limitations. For example, the discussion in appendix A on the error analysis is about the same length as the AIAA paper.

The authors of this technical memorandum acknowledge the following people for their significant efforts in the RCC testing and analyses: Ignacio Norman, Jesus Reyna, Jr., and Scott Christensen of Rockwell International; Neal Webster of Loral Vought; Jim Milhoan and Don Tillian of Johnson Space Center.

Contents

Tables

Contents
(continued)

Page

Figures

Contents
(continued)

Contents
(concluded)

Acronyms

atm	atmospheres
ACE	Aerotherm Chemical Equilibrium Program
ARMSEF	Atmospheric Reentry Materials and Structures Evaluation Facility
DTA	Double Type A
O.D.	outer diameter
RCC	reinforced carbon-carbon
RSI	reusable surface insulation
TEOS	tetraethyl-orthosilicate
TPS	thermal protection system

Introduction

The requirement for a reusable minimum weight thermal protection system (TPS) for the Space Shuttle Orbiter presented major material and design challenges. Ceramic materials were selected for most areas of the Orbiter external surface, but reinforced carbon-carbon (RCC) was selected for high-temperature regions where reusable surface insulation (RSI) could not safely be used as TPS. RCC has been successfully reused in these high-temperature regions on the Shuttle Orbiters since the first flight of the Columbia vehicle (April 1981).

Oxidation protection of the RCC material is accomplished in a three-step process. Initial protection is provided by converting the outer carbon surface to silicon carbide, SiC, in a diffusion coating process. Further oxidation resistance is obtained by impregnation with tetraethyl-orthosilicate (TEOS). When cured, TEOS leaves a silicon dioxide, SiO_2, residue throughout the coating and carbon substrate. The third step is the application of a surface sealant (Type A—sodium silicate/SiC mixture) to fill any porosity or micro cracks on the surface. Even with this oxidation protection system, the RCC material still loses mass over an extended temperature range without any apparent surface recession.

The most important parameter in the determination of RCC mission life is the oxidation of the carbon substrate which occurs as a result of oxygen penetrating the protective coating. The resultant strength degradation caused by substrate mass loss restricts the mission life capability since the RCC will be unable to sustain the imposed flight loads. Medford[1,2] developed analytical methods for predicting subsurface RCC oxidation performance including chemical kinetics at the subsurface oxidation sites, diffusion of oxygen into the coating fissures, growth of product film on the coating external surface and fissure walls, and differential thermal expansion between coating and substrate. These initial analyses used the experimental data of McGinnis[3] for a RCC material without TEOS and surface sealant. Subsurface mass loss testing for RCC impregnated with TEOS and the Type A surface sealant was conducted in 1984[4,5] and 1990[6] to develop mass loss correlations (radiant and convective) for predicting the mission life of Orbiters Columbia, Atlantis, and Discovery.

The RCC was originally developed to have nominal multi-mission capability with a maximum temperature of 1811 K (2800°F). However, the extended operational flight envelope of the Orbiter and abort conditions can result in RCC surface temperatures significantly higher than the original design value. Requirements to increase the Orbiter range capability during certain abort conditions result in predicted RCC surface temperatures in excess of 2088 K (3300°F), causing RCC surface recession. To quantify RCC performance over the range of temperatures and pressures for these abort conditions, an over-temperature test program[6] was conducted. This data was used by Curry[7] to establish a single mission limit RCC temperature. Thus, there has been an ongoing effort to characterize the oxidation performance of the RCC surface coating material at these higher temperatures.

A second application of the sodium silicate sealant (i.e., Double Type A [DTA]) was made to the RCC components installed on the Orbiter Endeavor to increase mission life by decreasing the subsurface oxidation. Subsequently, the test program has been expanded to characterize the oxidation performance of the RCC with the DTA sealant.[8]

Past efforts to characterize SiO_2/SiC/C systems have generally been conducted in a laboratory environment. This investigation differs from these efforts by analyzing the oxidation of the complex RCC material system in a high-temperature Arc-Jet air environment simulating flight entry conditions.

This paper uses data from the JSC over-temperature and DTA convective mass loss test programs to develop an analytical method for predicting the RCC sealant/coating (sodium silicate/SiC) erosion and substrate oxidation. A non-equilibrium, chemically reacting boundary layer program is used to predict Arc-Jet test and flight heating conditions. Utilizing the ablation model, correlated with Arc-Jet test data, mass loss predictions/mission life of the RCC oxidation protection coating are presented for typical flight entry conditions.

RCC Oxidation Tests

Successful RCC flight experience and an expanded operational flight envelope have led to higher heating rates and temperatures. An over-temperature test program has been conducted at these higher heating conditions to quantify RCC performance. This test program has provided the database to develop surface mass loss correlations.

DTA was applied to the RCC components installed on the Orbiter Endeavor as part of the baseline carbon system to further decrease subsurface mass loss and increase mission life. Orbiters Columbia, Atlantis, and Discovery also have select RCC components with DTA sealant as a result of replacement activity. Accordingly, the test program was expanded to characterize the increased oxidation protection of the RCC with the DTA sealant.

Test Specimens and Procedures

All test and calibration specimens were 7.1-cm (2.8 in.)-diameter 19-ply discs of RCC (figs. 1 and 2). The calibration specimens have three Type C (tungsten - 5% rhenium / tungsten - 26% rhenium) thermocouples installed as shown in figure 1. TC #1 and TC #3 sense front surface temperatures and TC #2 senses the back surface temperature.

Forty Double Type A specimens and four calibration models were available for testing. The specimens were fabricated from AVTEX RCC substrate:

- Coated/TEOS/Double Type A specimen: SiC-coated, impregnated with TEOS and sealed with DTA surface sealant enhancement.

Sixty-two test specimens and seventeen calibration models (instrumented with thermocouples) were available in the over-temperature test program. There were three classes of specimens which were fabricated from either AVTEX or ENKA RCC substrate:

- Coated/TEOS/Type A specimen: SiC-coated, impregnated with TEOS and sealed with Type A surface enhancement
- Coated/TEOS/No Type A specimen: SiC-coated, impregnated with TEOS, but not sealed with Type A surface enhancement
- Uncoated/TEOS specimen: RCC substrate, impregnated with TEOS

Test specimens were photographed, weighed, and thickness measurements made before and after testing. Specimens were handled with clean white gloves and weighed to within 0.1 mg. Aluminum bags were used to prevent absorption of atmospheric moisture while the specimens were being weighed. Before weighing, the specimens were placed inside aluminum bags that were then placed inside a 149°C (300°F) oven for four hours to remove water of hydration. The aluminum bags were then sealed and the specimens allowed to cool before weighing. After the specimens had been tested, they were cooled under vacuum in the test chamber for 25 minutes to minimize oxidation of the carbon substrate during repressurization.

Although the calibration models were instrumented with three Type C thermocouples, an optical pyrometer operating at 0.865 mm was also used as a secondary, non-intrusive surface temperature measuring device. During the calibration runs, the pyrometer matched the readings from the surface thermocouples with an emissivity correction factor to account for the window and the mirror loss of 0.68 as in previous RCC test programs.[6] The desired surface pressures in the test matrix were measured with a 10.03 cm O.D. water-cooled pressure model. The pressure model and the test specimen with holder have the same outside diameters.

The test program was performed in both test chambers of the Atmospheric Reentry Materials and Structures Evaluation Facility (ARMSEF).[9] Test gases (23% O_2 and 77 % N_2 by mass) are heated by a segmented, constricted arc heater and injected in a vacuum chamber through a water-cooled conical nozzle that has a 15° half angle. During testing, the chamber static pressure was kept below 40 Pa (0.3 millimeter of mercury). Desired test pressures were generated by the impact pressure of the hypervelocity flow field as verified by a 10.03-cm-O.D. water-cooled pressure model.

Test specimens were subjected to constant surface temperature heating cycles. In these heating cycles, by slightly varying the current to the arc heater, the surface temperature of the test specimens, as recorded by the optical pyrometer, was maintained at a pre-determined value.

Double Type A Tests

DTA tests were conducted at temperatures of 1533 K to 1811 K (2300°F to 2800°F) at stagnation pressures of 0.01 atm, 0.03 atm, 0.05 atm, and 0.07 atm (table I). The test conditions provide a wide range of temperature, at limited pressures, with which to evaluate surface sealant loss. Weight loss measurements were used to calculate mass loss rates for the various test conditions. Microscopic analyses were then used to estimate the surface sealant and SiC thicknesses. Test specimens were cross-sectioned to determine any subsurface oxidation. Photomicrographic examinations of the cross-sections of the DTA specimens revealed no substrate oxidation. Therefore, the mass loss rates determined from these tests are considered to be only surface sealant (Na_2SiO_3) loss. A photograph of a typical post-test DTA specimen showing the effects of surface melting and formation of SiO_2 beads on the surface can be seen in figure 3. In this figure the surface gives a wet/moist appearance similar to a mist spray forming beads of water on a freshly waxed surface.

Sealant loss rates, at constant pressures, are shown in figure 4 which is typical of an Arrhenius form of mass loss rate with the reciprocal of temperature. A definite dependency of pressure on the sealant loss is exhibited, therefore, the test data was correlated using the following equation,

$$\dot{m} = k\left(p / p_0\right)^n e^{-E/RT}, \tag{1}$$

where $\dot{m}$ is the mass loss rate per unit area, k is the pre-exponential coefficient in the same units as $\dot{m}$, E/R and T are units of temperature, p is the stagnation pressure, and p_0 is the reference pressure at 1 atm in the same units as p. This equation can be used for predicting sealant loss over the temperature range of 1533 K to 1811 K; 0.01 atm to 0.07 atm (table II).

Over-Temperature Test Results

Over-temperature tests were performed at the conditions shown in table III.[6] Negligible surface recession of the RCC SiC coating has been observed at temperatures below 1967 K (3080°F); however, between 1967 K and 2136 K (3080°F and 3385°F) a steady increase in the surface recession is observed. At 2136 K (3385°F), a SiC diffusion-limited erosion is observed.

The oxidation mechanisms observed during these high-temperature 1922 K to 2117 K (3000 to 3350°F) tests, follow the classic passive/active oxidation reactions as reported by Schiroky, Price, and Sheehan,[10] Rosner and Allendorf,[11] Gulbransen and Jansson,[12] and Strife[13] associated with sodium silicates, glass and SiC (fig. 5). A correlation of the RCC data delineating the passive/active regimes is compared with data from the literature. As a result of the TEOS impregnation and sodium silicate sealant, a protective SiO_2 film protects the SiC coating against active oxidation. As the temperature increases, SiO_2 melts and flows; SiO gas forms at the SiO_2-SiC interface and within the specimen. This activity dramatically increases at approximately 2061 K (3250°F), resulting in an eruption of bubbles on the specimen surface and mechanical disruption of the film. Exposure of the SiC then results in an aggressive active oxidation resulting in a coating breach and exposure of the bare carbon substrate. These complex high-temperature chemistry mechanisms are further complicated by corresponding changes in the material catalytic efficiency and emissivity of the RCC surface and TEOS impregnated substrate.

Sealant Loss: Weight loss and thickness measurements were used to calculate mass loss/surface recession rates for the various test conditions (table IIIa). The DTA tests provided sealant loss data for a temperature range of 1533 K to 1811 K. The over-temperature tests provide sealant loss data from 1867 K to 2033 K (2900°F to 3200°F). This sealant loss data (fig. 4) is somewhat higher than the DTA sealant loss data and does not appear to be pressure sensitive. This is a result of more aggressive melting/oxidation reactions on the RCC surface at these higher temperatures. A photograph of a post-test specimen showing the sealant loss surface effects can be seen in figure 6 where beads of SiO_2

formed and rivulets swept from the stagnation region to the outer edge. Sealant loss in this temperature range has been correlated using Eq. (1) and the coefficients given in table II. Predicted sealant recession depth can be computed using these coefficients and the sealant density of 1.730 gm/cm^3.

Coating Recession: SiC recession rate calculations were made using three test parameters: temperature, pressure and time duration, and pre- and post-test coating thickness measurements at several locations on the test specimens (table IIIb). Determination of the time duration of the coating breach (SiC loss) was made using the recorded temperature time history. SiC coating recession rate was calculated by dividing the coating loss by time duration. Figure 7 is a plot of the normalized recession rate variation with reciprocal of temperature (i.e., Arrhenius form). As previously discussed, the recession rate is negligible for temperatures less than 1967 K (3080°F); between 1967 K and 2136 K (3080°F to 3385°F), a steady increase in recession rate is observed. A photograph of a post-test specimen representative of a rate controlled reaction is shown in figure 8. For this test condition the SiC coating is still protecting the RCC substrate. At 2136 K (3385°F) a constant recession rate occurs independent of surface temperature, and exhibits a diffusion-limited behavior (fig. 9). In this figure it can be seen that the sealant has been removed and most of the coating has been eroded in the stagnation region and active oxidation of the carbon substrate (the black region) is in progress. Coating mass loss has been correlated with Eq. (1) and the coefficients shown in table II. Predicted coating recession depth can be computed using these coefficients and the coating density of 2.114 gm/cm^3.

Substrate recession: An extensive literature database, both analytical and experimental, exists for the oxidation characteristics of bare carbon. Initial oxidation studies by Scala[14] were used to estimate the reaction rate/diffusion limits. Therefore, the objective of this test series was the determination of the RCC substrate recession rate once the SiC coating had been depleted and the substrate was directly exposed to the oxidizing environment.

Specimens were tested over a temperature range of 1033 K to 2144 K (1400°F to 3400°F) (table IIIc). Since oxidation of the RCC substrate is initiated at a relatively low temperature, it was important to minimize this oxidation during the initial temperature transient. This was accomplished by using 100% nitrogen test gas during the initial transient period followed by an instantaneous switch to air test gas. Surface recession rate data exhibits a well-defined reaction rate, but the expected diffusion limit at the higher temperature is not as well-defined due to the RCC substrate being impregnated with TEOS (fig. 10). This data was correlated with Eq. (1) and the coefficients given in table II. Predicted substrate recession depth can be computed using these coefficients and the substrate density of 1.362 gm/cm^3. The pre-test and post-test photographs of a RCC substrate specimen are shown in figure 11. In the pre-test photograph the fabric weave is clearly illustrated, while in the post-test photograph the weave pattern is less distinct and the oxidation effects on the carbon surface are clearly evident.

Analysis Results

Predictions of sealant loss, SiC and bare RCC mass loss are compared to plasma Arc-Jet test results, thermochemical ablation theory, and for typical Orbiter entries. An error analysis of the correlations for the sealant, SiC coating, and RCC substrate are presented in appendix A.

Plasma Arc Tests

Equilibrium stagnation heating was calculated using the stagnation enthalpy, pressure, and pressure distribution. Adjustments were made to the stagnation enthalpy to match the measured heating rates. The effective radius was corrected from 5.08 cm to 16.764 cm using the method described by Hiester and Clark[15] to correct the heating from a hemispherical body to a blunt axisymmetric body. The equation used is given as

$$R_{Effective} = R_{Hemisphere} = 3.3\ R_{Flat\ Face} \qquad (2)$$

The modified version of the BLIMP program[16] with the built-in radiation equilibrium iteration procedure[17] was used for these calculations. The results of this calculation using the RCC emissivity provided excellent approximations to the reported calorimeter heating.

Since the excellent agreement between the predicted heating for equilibrium flow and the calorimeter data were obtained, the same stagnation conditions were used for heating conditions for non-equilibrium flow. Sambamurthi's[18] upper limit curve fits to the NASA/Ames recombination coefficient data[19] for surface catalysis for reaction cured glass as reported by Rochelle[20] were used in this calculation. The calculation method used in the present work uses a 5-species (N, O, NO, N_2, O_2) air model with equilibrium edge conditions.

Three over-temperature test conditions have been selected to compare predicted RCC response with test data:

- IN-06, 2117 K, 0.048 atm
- IN-20, 2100 K, 0.160 atm
- AU-05, simulated Orbiter abort condition

Figure 12 shows the predicted heating and corresponding measured and predicted surface temperature for test IN-06. In this figure, abrupt changes in the correlated heating rate indicate the various states of thermochemical activity. Predicted mass loss, shown in figure 13, consists of sealant loss followed by SiC erosion. The endothermic and exothermic behavior of sealant and SiC erosion processes are obvious. The correlated heating rate during sealant loss is approximately 60% of the BLIMP heating for non-equilibrium flow while, during SiC erosion, the correlated heating is approximately 18% higher than the BLIMP heating for non-equilibrium flow. These heating variations are attributed to surface chemical reactions, wall emissivity, and surface catalytic effects. Predicted mass loss is compared to the test data using two approaches: coating thickness and weight loss measurements. Measured mass loss using coating thickness compares well with prediction (fig. 13a); mass loss using weight change results shows a conservative prediction of the mass loss (fig. 13b). This is not unexpected since the maximum coating thickness erosion was used in the calculation of measured mass loss and the weight change is an average over the entire specimen. This is better illustrated in figure 14 which shows the surface of IN-06 after testing. This figure shows the dry SiC surface as a result of sealant loss and the initial heating of the underlying RCC substrate due to SiC erosion. For this test the stagnation point heating was slightly off center.

Figure 15 shows the predicted heating and corresponding measured and predicted surface temperature for test IN-20. In this figure abrupt changes in the correlated heating rate again indicate the various states of thermochemical surface activity, similar to that observed in figure 12. Predicted mass loss, shown in figure 16, consists of sealant loss, SiC erosion, and RCC substrate ablation. Three distinct correlated heating zones for this test are shown: sealant loss, SiC erosion, and substrate ablation. Once again during sealant loss, the convective heating is less ($\approx$ 60%) than the BLIMP non-equilibrium value and the correlated heating greater than non-equilibrium during the SiC ($\approx$ +10%) and substrate erosion ($\approx$ +15%). These heating variations are attributed to surface chemical reactions, wall emissivity, and surface catalysis. Predicted mass loss (fig. 16) compares favorably with measured mass loss using both thickness (fig. 16a) and weight change measurements (fig. 16b). This is better illustrated in figure 17 which shows the surface of IN-20 in the coated graphite holder after testing. This figure shows the outer edge dry SiC coating/RCC substrate interface, and the effects of the more aggressive erosion due to carbon oxidation in the center of the model.

Figure 18 shows the predicted heating and corresponding measured and predicted surface temperature for test AU-05, which simulated a typical abort condition. Predicted recession depths and mass loss, shown in figure 19, consist of sealant and SiC loss. Once again during sealant loss, the convective heating is less ($\approx$ 60%) than the BLIMP non-equilibrium value. The heating variations are attributed to surface chemical reactions, wall emissivity, and surface catalysis. The recession depth (fig. 19a) is within 33%, 23%, and -2.3% of the thickness change measurements reported by JSC, Loral, and Rockwell, respectively.[21] The predicted mass loss is conservatively estimated when compared with measured mass loss (fig. 19b) by over 160%. A photograph of the post-test surface is shown in figure 20. This figure illustrates the uneven erosion similar to that for IN-06, but also shows a mottled effect indicating more aggressive oxidation of the SiC coating during the diffusion-limited erosion.

Thermochemical Ablation Theory

Thermochemical ablation for the oxidation-protected RCC is compared with data obtained from the Arc-Jet plasma tunnel. The computer code used herein is the Aerotherm Chemical Equilibrium (ACE) Program.[22] This program solves for surface elemental mass balances, producing solutions for ablation rate normalized by mass-transfer coefficient in terms of pressure, surface temperature, and normalized pyrolysis gas rate. A variety of physicochemical models can be assumed, including consideration of equilibrium or rate-controlled reactions at the surface and mechanical removal of candidate surface species.

An open system analysis was performed for a sodium silicate system with 30 species at conditions corresponding to the DTA test pressures. The species selected were based on Na, Si, C, O, and N atoms. The boundary layer consists of 78% N and 22% O (with a small fraction of C) with two parts sodium and one part Si for three parts O (Na_2SiO_3) for the char material. The pyrolysis gas rate was set to zero, since sodium silicate does not decompose in depth, but either melts or vaporizes. Non-dimensional char rates,

$$B'_c = \dot{m} / (\rho_e u_e C_M), \tag{3}$$

were varied from 1 to 10^{-10} for this analysis. (The subscripts c and e refer to char and edge conditions, respectively. C_M is the mass transfer coefficient while m, r, and u refer to the mass, density, and velocity, respectively.) ACE is limited to a single condensed species. The results presented in figure 21 indicate that the assumptions for chemical equilibrium below 2500 K are not accurate. Data from the DTA and over-temperature tests[6, 8] are shown in figure 21 compared to the ACE predicted data, but the predictions are in poor agreement for low temperature (1500 K to 2033 K) convective ablation data.

These results were as expected since there is no chemical means for removing Na_2SiO_3 from the surface until the temperature is sufficiently high that decomposition takes place. There are reasons that one might expect at least some mechanical removal of the sealant at surface temperatures below 2500 K. First, the sodium silicate melts at lower temperatures, and there will be some removal by liquid-layer flow. The loss of sealant in this manner was observed in the videos of tests, and liquid globules were found on the surface after cool down (figs. 3 and 6). The use of an artificial fail temper-ature for Na_2SiO_3 in ACE would be required to predict sealant loss in the low temperature regime; therefore Arrhenius equations were developed to predict sealant erosion for the surface temperature range 1500 K to 2033 K.

In a similar manner, ACE predictions were made for a SiC surface. Figure 22 compares the test data with ACE predictions. Once again, the dominant effect of the SiO, SiO_2, and Si species on the SiC mass loss rate is apparent. Only at the higher temperature ($\approx$ 2060 K)—where the test data indicate a SiC diffusion limit—do the ACE predictions agree with the test data.

The third stage of the oxidation-protected RCC material ablation is bare carbon-carbon recession. ACE predictions for pure carbon are compared with bare RCC recession in figure 23. The incorporation of TEOS into the RCC substrate inhibits the carbon oxidation at the lower temperatures, but reasonable agreement with ACE and diffusion limit theory is obtained at the higher temperatures.

In summary, while thermochemical ablation, as predicted by ACE, does not accurately predict the ablation performance of the oxidation protected RCC, the general mass loss rate trends are reasonably predicted.

Flight Predictions

The single mission limit and/or reusability of the RCC components can now be predicted using sealant, coating, and bare carbon-carbon correlations. Mission life predictions require an additional equation to predict subsurface oxidation.[7] Therefore, we will restrict these predictions to sealant loss and SiC erosion. The thermophysical properties used in this analysis can be found in appendix B.

Routine Shuttle Orbiter entries have little or no surface recession. However, extension of the Orbiter flight envelope certification to high inclination, heavy weight, and abort entries results in high surface temperatures (> 1867 K). Typical temperature/pressure profiles for a nominal and heavy weight entry are shown in figures 24 and 25. The higher surface temperature associated with heavy weight entry results in a greater sealant loss. A sketch showing the location of panel 9 on the Orbiter wing leading edge can be seen in figure 26. Predicted sealant loss for nominal and heavy weight entry is shown in table IV. Using these calculations, it takes approximately 9 heavy weight and 12 nominal entries to remove a 2-mil surface sealant thickness. Postflight inspection of the Orbiter Columbia indicate local loss of surface sealant after 12 flights, which is consistent with the predictions. However, minimal surface recession is predicted using the correlations, which is consistent with a passive state of SiC oxidation during entry (fig. 27).

Abort entries, resulting from main engine failure, result in even higher surface temperatures. Temperature/pressure profiles for a single-engine-out abort are shown in figure 28. Using this data, the corresponding surface sealant erosion has been predicted. As seen in table IV the surface sealant is ablated, but very little surface recession has occurred. These results show that a single-engine-out abort can be safely flown, but RCC refurbishing would be required before the next flight.

The results shown in table IV for these three trajectories were made assuming the general equation for prediction of sealant loss. Appendix A discusses in detail an error analysis for the sealant, SiC, and bare carbon substrate mass loss correlations. A review of the error bands shown in this appendix indicate less error when using the specific correlations. Accordingly, the mass loss for the trajectories shown in figures 24, 25, and 28 have been calculated using the specific correlations, and these results are shown in table V. As can be seen from these tables, the general equation predicts sealant protection for one more flight than does the specific equation predictions for a sealant thicknesses of 0.00508 cm for the heavy weight mission. There is a slight difference between the two methods in predicting the mission life for the abort mission even though over 94% of the sealant erosion is due to the over-temperature sealant loss, which is more aggressive than DTA sealant loss.

A better comparison between the two methods for predicting sealant loss can be seen by examining the predicted surface recession for each of the trajectories analyzed. The predicted sealant loss as a function of time for the two methods for a nominal mission can be seen in figure 29. This figure illustrates that the specific equation is slightly more conservative than the general equation over the entire trajectory, however the predicted surface recession is essentially the same after 1000 seconds. The variations between the two methods are in agreement with the error analysis presented in appendix A, and not unexpected due to the time spent in the 0.03 atm to 0.05 atm pressure range. Of slightly greater interest is the comparison of the predicted sealant loss for the heavy weight mission (fig. 30). In figure 30 it can be seen that the two methods are in agreement over the entire trajectory until the pressure exceeds 0.07 atm. The higher sealant loss predicted by the specific equations is due to calculations made using the 0.07 atm correlation, since no extrapolation is made for pressures outside the available data range (0.01 atm to 0.07 atm). This restriction is not imposed on the general equation. The predicted sealant loss for the abort mission can be seen in figure 31. Over 94% of the predicted sealant loss for the abort mission is due to using the over-temperature sealant correlation. At 380 seconds, the DTA sealant loss correlation becomes active until approximately 600 seconds into the entry when the mass loss rate becomes negligible. As with the heavy weight mission, the difference between the predicted sealant loss by the specific equations and the general equation is due to the no-extrapolation limitation imposed on the specific equation where the pressure is greater than 0.07 atm. Thus, the restriction on the specific equation provides a more conservative prediction to flight data than does the general equation. However, the predictions using the general equation can be used with confidence for flight predictions.

Summary

The RCC material has demonstrated outstanding high-temperature thermal structural characteristics during its application to the leading edge structural system for the Space Shuttle Orbiter.

Oxidation performance testing of the RCC in plasma Arc-Jet heating facilities was conducted to develop surface sealant (Type A) mass loss correlations. Over-temperature testing was performed to establish coating (SiC) recession for temperatures in excess of the multi-mission temperature limit. The resulting

database and correlations have been successfully applied in extending the Orbiter flight envelope and ensuring safety of flight for off-nominal (abort) entries.

Based on the ground test results, correlations/analyses, and flight performance, the Orbiter RCC system is expected to achieve its full mission life objectives and retain an over-temperature capability for potential mission abort conditions.

References

1. Medford, J. E.: Prediction of Oxidation Performance of Reinforced Carbon-Carbon Material for Space Shuttle Leading Edges, AIAA 75-730, Presented at the 10th Thermophysics Conference.

2. Medford, J. E.: Prediction of In-Depth Oxidation Distribution of Reinforced Carbon-Carbon Material for Space Shuttle Leading Edges, AIAA 77-783, Presented at the 12th Thermophysics Conference.

3. McGinnis, F. K.: Shuttle LESS Subsurface Attack Investigation Final Report, Report No. 221RP00241, Vought Corp., Dallas, TX, 1974.

4. Webster, C. N.: March 1984 Radiant Mass Loss Correlation—RCC/Coated/TEOS/Type A, Dir. No. 3-53200/RCC/4-003, Vought Corp., Dallas, TX, March 1984.

5. Webster, C. N.: June 1984 Convective Mass Loss Correlation—RCC/Coated/TEOS/Type A, Dir. No. 3-53200/RCC/4-006, Vought Corp., Dallas, TX, June 1984.

6. Milhoan, J. D.; Pham, V. T.; and Yuen, E. H.: Compilation of Reinforced Carbon-Carbon Transatlantic Abort Landing Arc Jet Test Results, NASA TM 104778, December 1993.

7 Curry, D. M.; Yuen, E. H.; Chao, D. C.; and Webster, C. N.: Space Shuttle Orbiter Carbon-Carbon Oxidation Performance, AD-Vol. 25-1, Damage and Oxidation Protection in High Temperature Composites, Vol. 1, pp. 47-64, ASME, 1991.

8. Milhoan, J. D. and Pham, V. T.: Double Type A Reinforced Carbon-Carbon Convective Mass Loss, JSC Thermal Branch Report JSC 26651, May 1994.

9. Rochelle, W. C.; Battley, H. H.; Tillian, D. J.; Grimaud, J. E.; Murray, L. P.; Lueke, W. J.; and Heaton, T. M.: Orbiter TPS Development and Certification Testing at the NASA/JSC 10 MW Atmospheric Reentry Materials and Structures Evaluation Facility, AIAA Paper AIAA-83-0147, presented at AIAA 21st Aerospace Sciences Meeting, Reno, Nevada, Jan. 10-13, 1983.

10. Schiroky, G. H.; Price, R. J.; and Sheehan, J. E.: Oxidation Characteristics of CVD Silicon Carbide and Silicon Nitride, Report No. GA-A18696, GA Technologies, 1986.

11. Rosner, D. E. and Allendorf, H. D.: High Temperature Kinetics of the Oxidation and Nitridation of Pyrolytic Silicon Carbide in Dissociated Gases, *The Journal of Physical Chemistry*, Vol. 74, No. 9, 1970, pp. 1829.

12. Gulbransen, E. A. and Jansson, S. A.: The High-Temperature Oxidation, Reduction and Volatilization Reactions of Silicon and Silicon Carbide, *Oxidation of Metals*, Vol. 4, No. 3, 1972, pp. 1972.

13. Strife, J. R.: Development of High Temperature Oxidation Protection for Carbon-Carbon Composites, Report No. NADC-91013-60, United Technologies Research Center, 1990.

14. Scala, S. M. and Gilbert, L. M.: Sublimation of Graphite at Hypersonic Speeds, *AIAA Journal*, Vol. 3, pp. 1635.

15. Hiester, N. K. and Clark, C. F.: Feasibility of Standard Evaluation Procedures for Ablating Materials, NASA CR-379, February 1966.

16. Murray, A. L.: Further Enhancements of the BLIMP Computer Code and User's Guide, AFWAL-TR-88-3010, June 30, 1988.

17. Williams, S. D.: Group 16 Iteration Procedure, Presented at the BLIMP Users Workshop, Houston, TX, April 14, 1993.

18. Sambamurthi, J.: Undocumented communication at AFE telecon with W. C. Rochelle, June 6, 1991.

19. Kolodziej, P. and Stewart, D. A.: Nitrogen Recombination on High Temperature Reusable Surface Insulation and the Analysis of its Effect on Surface Catalysis, AIAA Paper AIAA-87-1637, presented at AIAA 22nd Thermophysics Conference, Honolulu, Hawaii, June 8-10, 1987.

20. Rochelle, W. C. and An, M. Y.: Leading Edge Structural Subsystem (LESS) Entry Heating Study-Final Report, Volume I-Methodology and Results, LESC-30453, Lockheed Engineering & Sciences Company, Houston, TX, May 1993.

21. Webster, C. N.: RCC Recession Rates from Over-Temperature Test Data, Dir. No. 3-56700/RCC/1-0001, Vought Corp., Dallas, TX, May 1991.

22. Anonymous, User's Manual for Aerotherm Chemical Equilibrium Computer Program (ACE 81), UM-81-11/ATD, Acurex Corp., Mountain View, CA, Aug. 1981.

Table I DTA Sealant Test Conditions and Mass Loss

Stag. Pressure atm	Pyrometer Temperature K	Specimen	Time Hours	Mass Loss gm	Stag. Pressure atm	Pyrometer Temperature K	Specimen	Time Hours	Mass Loss gm
0.07	1811	1B23	8	0.100	0.05	1922	1B15	4	1.688
		2B23	8	0.069			2B15	5	2.166
	1756	1B21	8	0.002		1811	1A23	8	0.568
		2B21	8	0.016			2A23	8	1.211
	1700	1B19	8	0.011		1756	1A21	6	0.132
		2B19	8	0.021			2A21	6	0.185
	1644	1B17	8	0.007		1700	1A19	8	0.085
		2B17	8	0.009			2A19	8	0.082
						1644	1A17	9	0.088
0.03	1811	1B22	5	0.822			2A17	8	0.103
		2B22	5	0.749		1533	1A15	5	-0.008
	1756	1A22	5	0.270			2A15	6	0.054
		2B20	5	0.258					
	1700	1B18	8	0.204	0.014	1700	1A18	6	0.803
		2B18	8	0.208			2A18	6	0.695
	1644	1B16	8	0.014		1644	1A16	6	0.385
		2B16	8	0.021			2A16	6	0.411
	1533	1B14	8	-0.011	0.01	1533	1A14	8	0.168
		2B14	8	0.016			2A14	8	0.230

Table II Arrhenius Equation Constants

Description		k	-E/R	n	Temperature Range	
		gm/cm^2-hr	K		low K	high K
Sealant	DTA general	7.17822×10^3	-41421.7	-2.4108	1533	1922
	0.010 atm	4.5008×10^8	-41421.7	0.0	1533	1811
	0.014 atm	1.3047×10^8	-41421.7	0.0	1533	1811
	0.030 atm	2.6014×10^7	-41421.7	0.0	1533	1811
	0.050 atm	2.6014×10^7	-41421.7	0.0	1533	1922
	0.070 atm	2.2590×10^6	-41421.7	0.0	1533	1811
Sealant	Over-Temperature	1.58949×10^{11}	-54623.2	0.0	1908	2117
SiC	Diffusion	1.71227×10^1	0.0	0.0	2136	2478
	Rate	1.06363×10^{47}	-225226.9	0.0	1967	2136
	Low Temperature Cutoff	1.84630×10^{-3}	0.0	0.0	1811	1967
Carbon	Rate	1.57251×10^3	-8085.9	0.5	1056	1867
	Diffusion	2.02865×10^1	0.0	0.5	1867	2478

Table IIIa Sealant Over-Temperature Test Conditions and Mass Loss

Specimen	Pyrometer Temperature K	Stag. Pressure atm	Time Seconds	Mass Loss gm
IN-14	2050	0.146	223	0.660
IN-28	2047	0.147	900	5.091
2	2033	0.049	330	1.643
AB-16	2033	0.049	330	1.244
18	2033	0.083	330	1.737
14	2033	0.083	600	2.093
5	2033	0.151	330	2.108
IN-22	2022	0.143	330	0.392
AB-15	1978	0.043	330	0.628
AC-22	1978	0.047	3300	2.730
4	1956	0.151	330	0.551
3	1922	0.076	330	0.358
16	1922	0.076	800	0.810
AB-13	1908	0.045	353	0.303

Table IIIb SiC Over-Temperature Test Conditions and Recession Depth

Specimen	Pyrometer Temperature K	Stag. Pressure atm	Sealant Start Time sec	SiC Start Time sec	SiC End Time sec	Test End Time sec	Recession Depth cm
IN-06	2117	0.048	18	42	74	74	0.067
IN-12	2061	0.150	17	114	150	330	0.085
IN-08	2089	0.154	16	79	110	110	0.076
IN-18	2089	0.154	25	72	105	330	0.080
IN-29	2117	0.154	22	102	132	132	0.061
IN-04	2111	0.159	12	44	74	74	0.084
IN-20	2100	0.160	12	43	82	95	0.083
IN-26	2117	0.160	13	19	64	65	0.072
AT-15	2117	0.160	14	53	87	87	0.083
IN-23	2061	0.148	22	70	900	900	0.022
IN-14	2050	0.146	22	77	223	223	0.018
IN-19	2050	0.142	22	77	3600	3600	0.047
IN-21	2033	0.138	22	90	1200	1200	0.032
IN-25	2033	0.050	22	90	3600	3600	0.020
IN-22	2022	0.143	22	102	330	330	0.003
389E04	1811	0.050	20	2620	28800	28800	0.008
TA3-02	1811	0.050	20	2620	28800	28800	0.005

Table IIIc RCC Carbon Substrate Over-Temperature Test Conditions and Recession Depth

Specimen	Temperature K	Stag. Pressure atm	Test Time sec	Recession Depth cm
28	1056	0.035	4500	0.099
27	1256	0.047	525	0.084
25	1256	0.091	600	0.104
26	1444	0.098	500	0.157
IN-34	1478	0.050	600	0.196
32	1644	0.047	400	0.269
IN-31	1711	0.085	330	0.218
NH-7	1728	0.142	300	0.241
23	1839	0.028	180	0.140
29	1867	0.047	200	0.180
IN-30	2011	0.142	153	0.208
IN-24	2106	0.147	150	0.239
NH-8	2144	0.142	120	0.193

Table IV RCC Sealant Mass Loss Predictions for Atmospheric Reentry Flight Environments on the Wing Leading Edge Panel 9 Using the General Equation

		Sealant Mission Life (No. of Flights)		
Type of Flight Trajectory	Sealant Loss Per Flight cm/flight	Sealant Thickness 0.00254 cm	Sealant Thickness 0.00381 cm	Sealant Thickness 0.00508 cm
Nominal (STS - 30)	.00035523	6	9	12
Heavy Weight	.00050458	4	6	9
Transoceanic Abort Landing	.00348873	Less Than One	1	1

Table V RCC Sealant Mass Loss Predictions for Atmospheric Reentry Flight Environments on the Wing Leading Edge Panel 9 Using the Specific Equations

		Sealant Mission Life (No. of Flights)		
Type of Flight Trajectory	Sealant Loss Per Flight cm/flight	Sealant Thickness 0.00254 cm	Sealant Thickness 0.00381 cm	Sealant Thickness 0.00508 cm
Nominal (STS - 30)	.00040317	6	9	12
Heavy Weight	.00061963	4	6	8
Transoceanic Abort Landing	.00361164	Less Than One	1	1

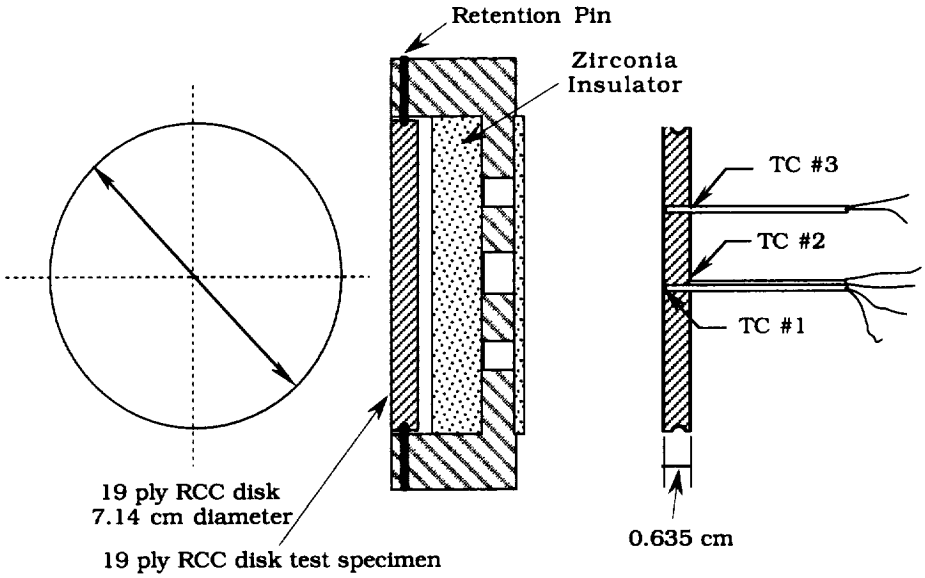

Fig. 1 Test Configuration With the RCC Test Specimen Installed in the Model Holder.

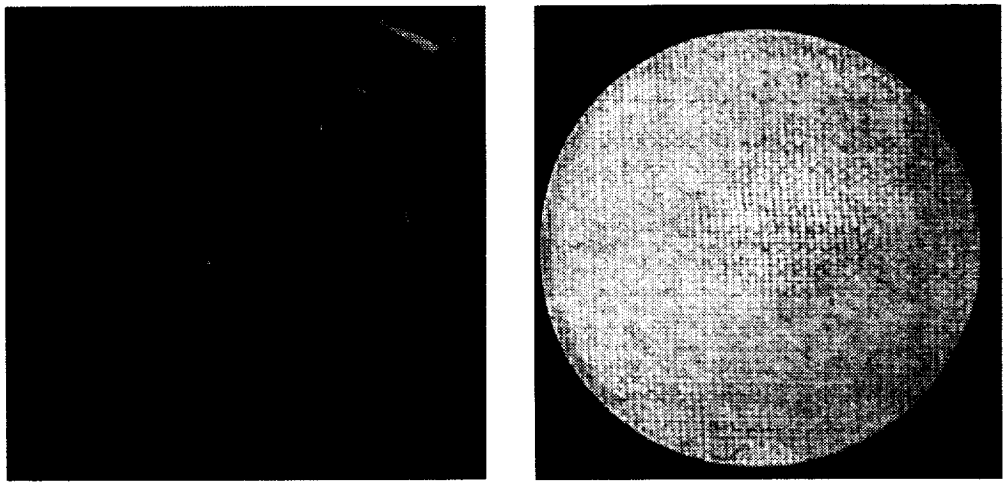

Fig. 2 Pre-Test Specimen Installed in the Coated Graphite Holder.

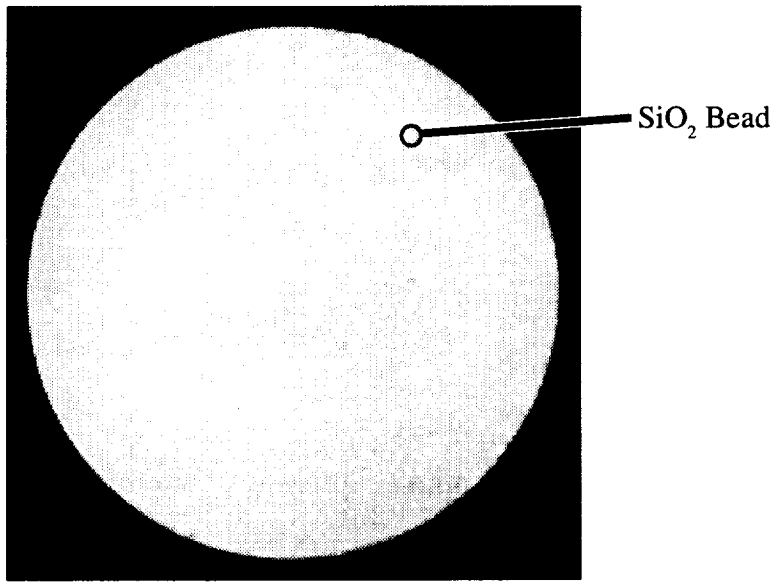

Fig. 3 Post-Test DTA Sealant Showing Effects of Surface Melting/SiO_2 Bead Formation.

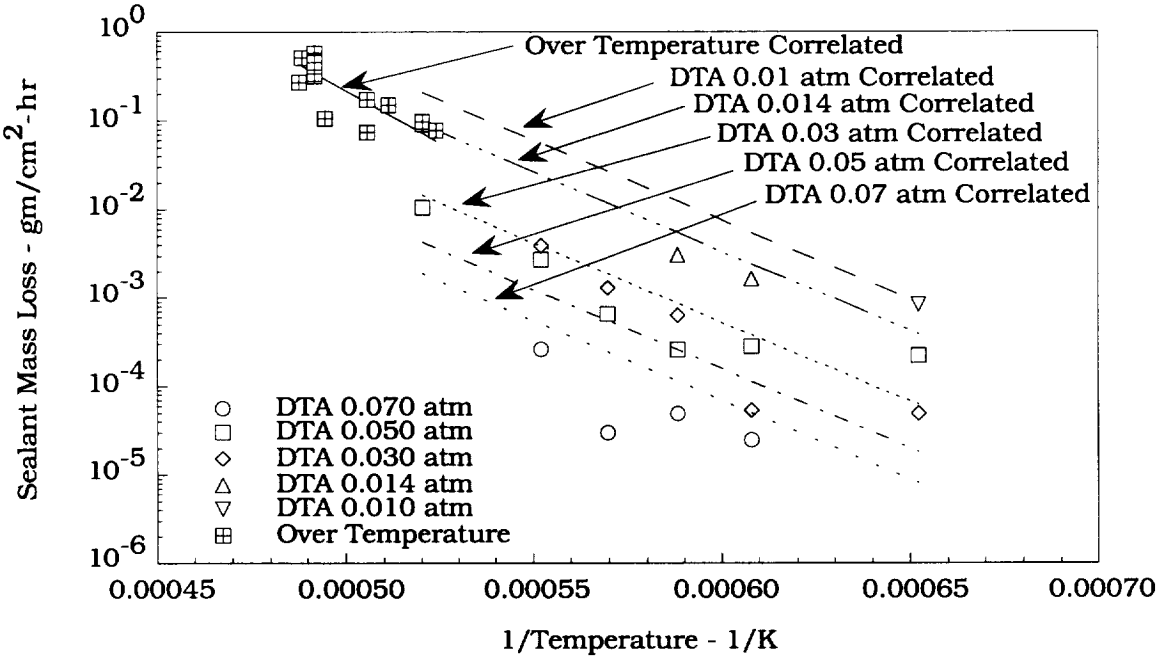

Fig. 4 DTA & Over-Temperature Sealant Experimental Mass Loss Rate Data Compared to Correlated Mass Loss Rates.

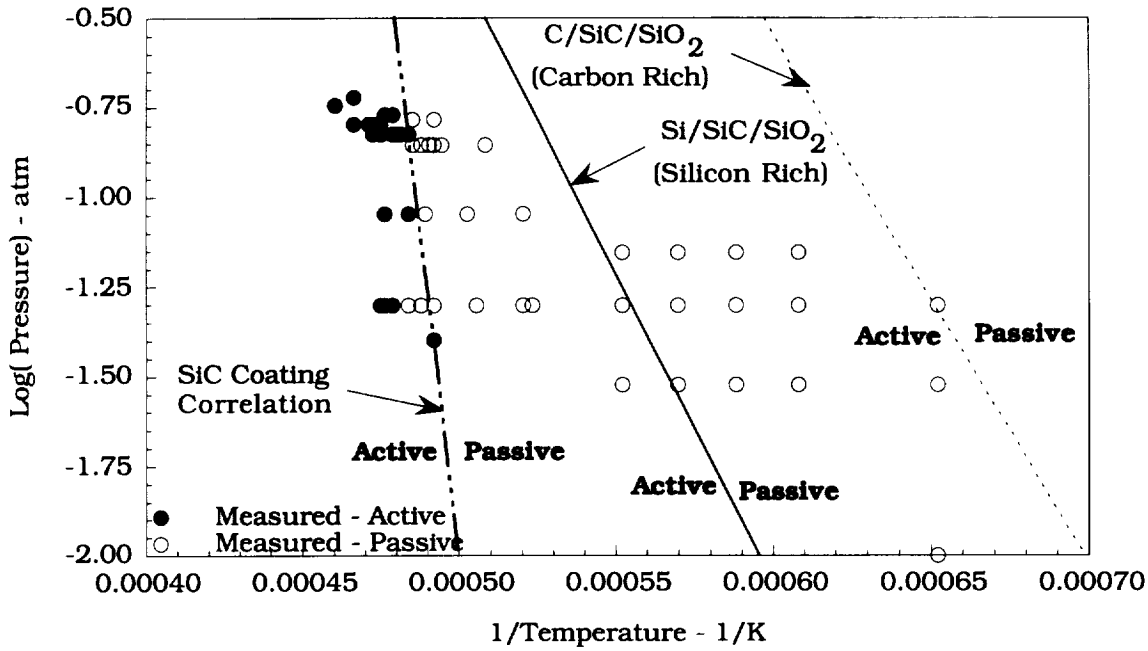

Fig. 5 Comparison of RCC Test Data With Two Equilibrium Conditions for Silicon Carbide With Carbon or Silicon Rich.

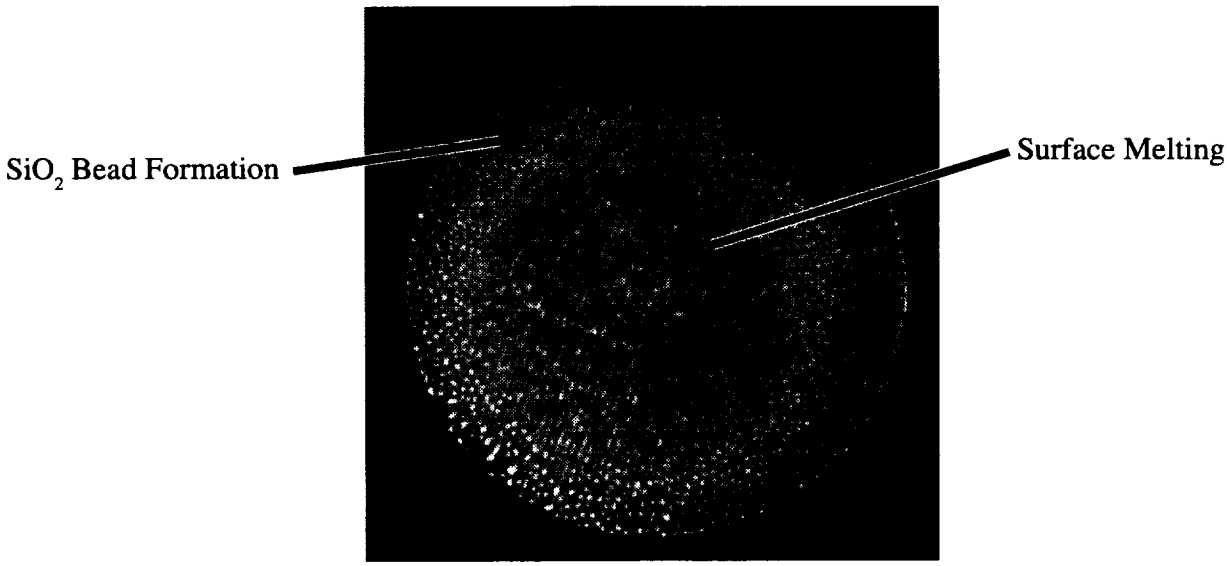

Fig. 6 Post-Test TAL (Over-Temperature) Sealant Showing Effects of Surface Melting and SiO_2 Bead Formation.

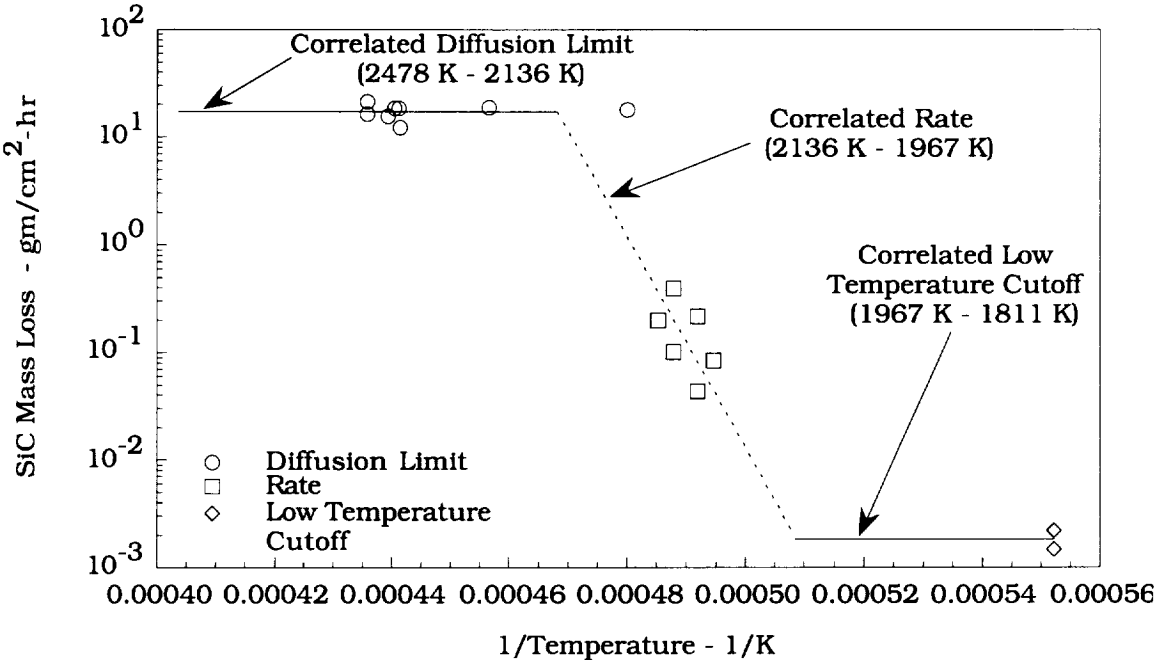

Fig. 7 SiC Coating Experimental Mass Loss Rate Data Compared to Correlated Mass Loss Rates.

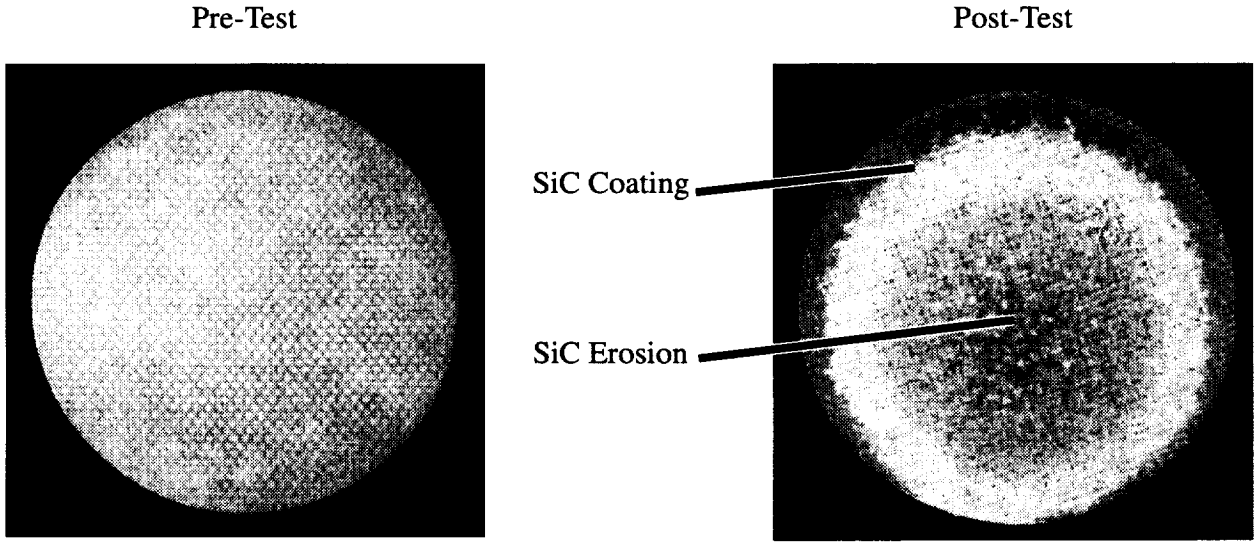

Fig. 8 Post-Test Photograph Showing SiC Surface Coating From the SiC Rate-Controlled Test.

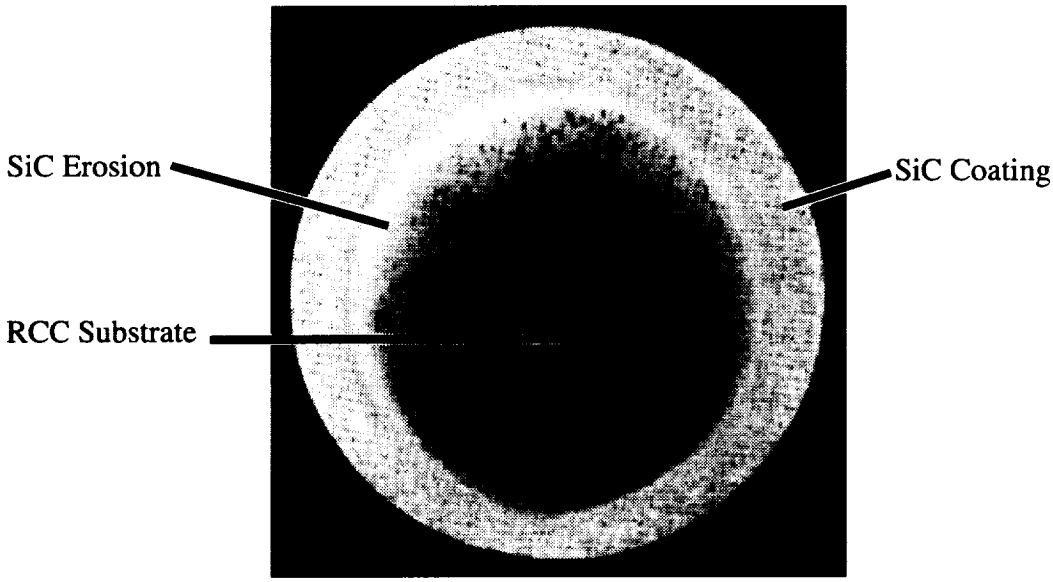

Fig. 9 Post-Test Photograph Showing the Surface After an Over-Temperature SiC Diffusion-Limited Test.

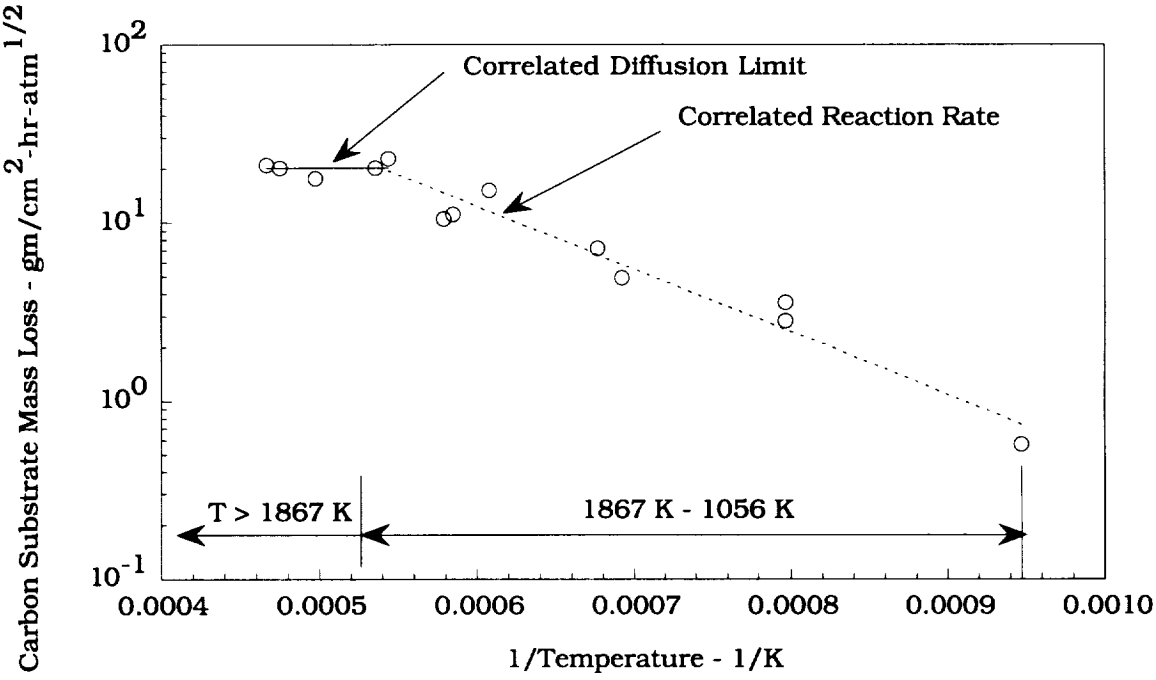

Fig. 10 RCC Carbon Substrate Experimental Mass Loss Rate Data Compared to Correlated Mass Loss Rates.

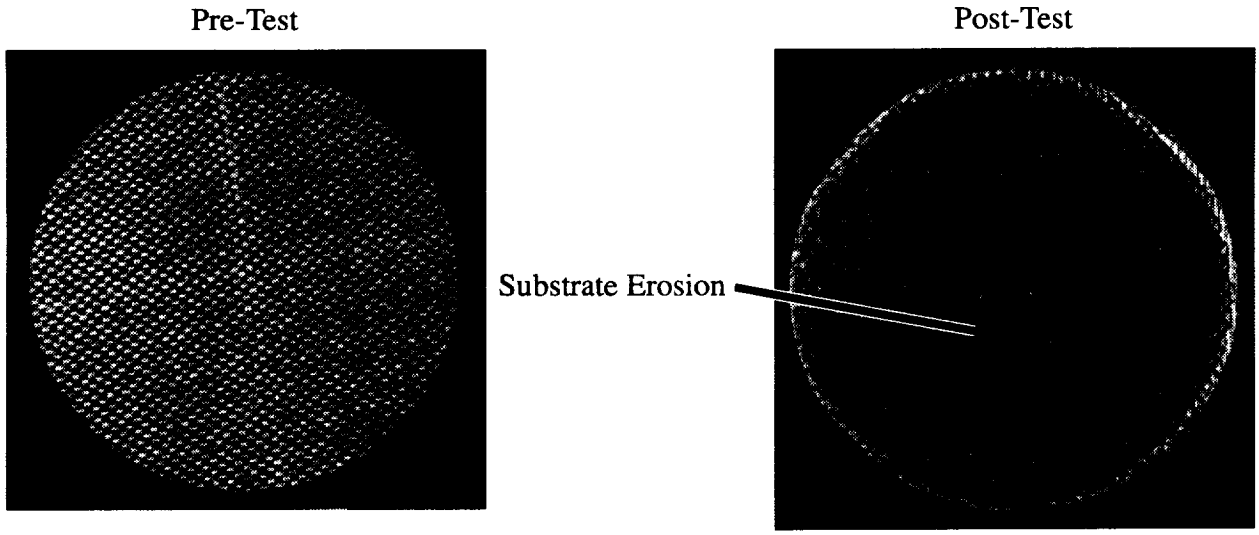

Fig. 11 Photograph Showing the Pre-Test RCC Substrate Virgin State and Post-Test RCC Substrate Oxidized State.

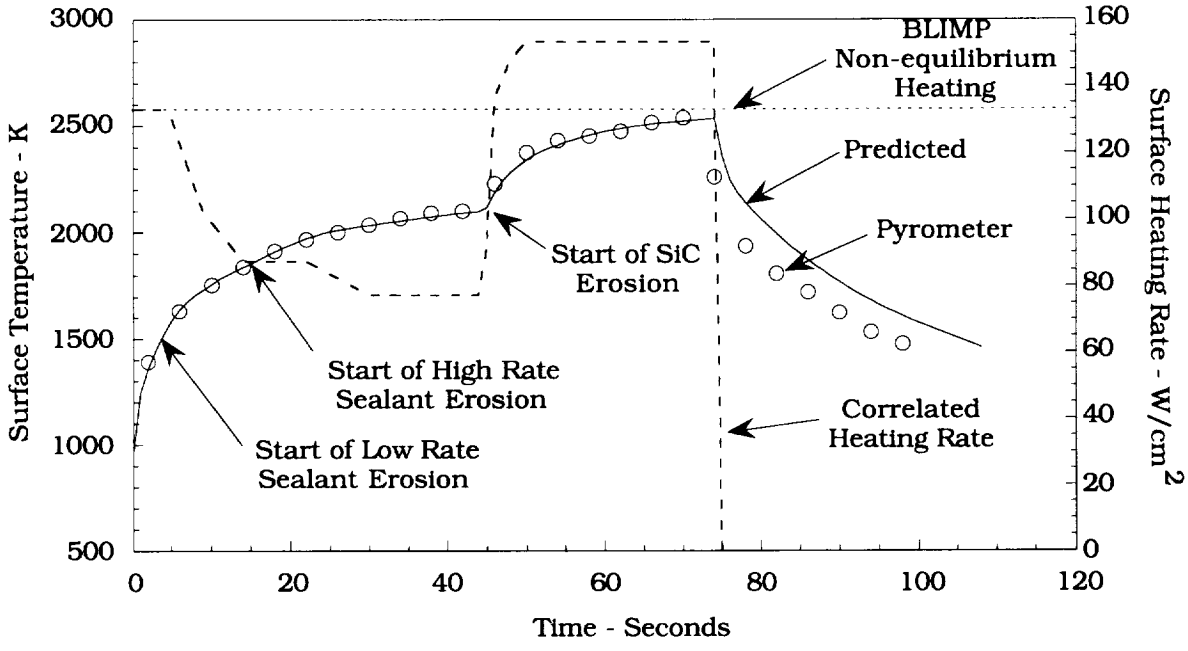

Fig. 12 Comparison Between Predicted and Experimental Surface Temperatures and Heating Rates for IN-06.

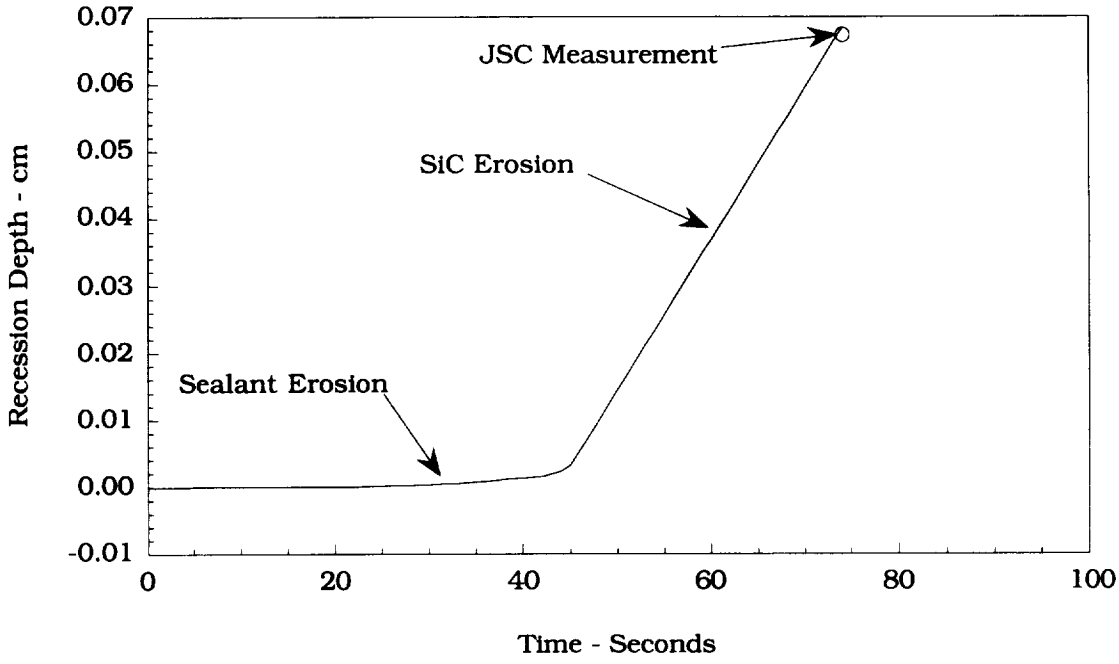

Fig. 13a Predicted Recession Depth Time History for IN-06.

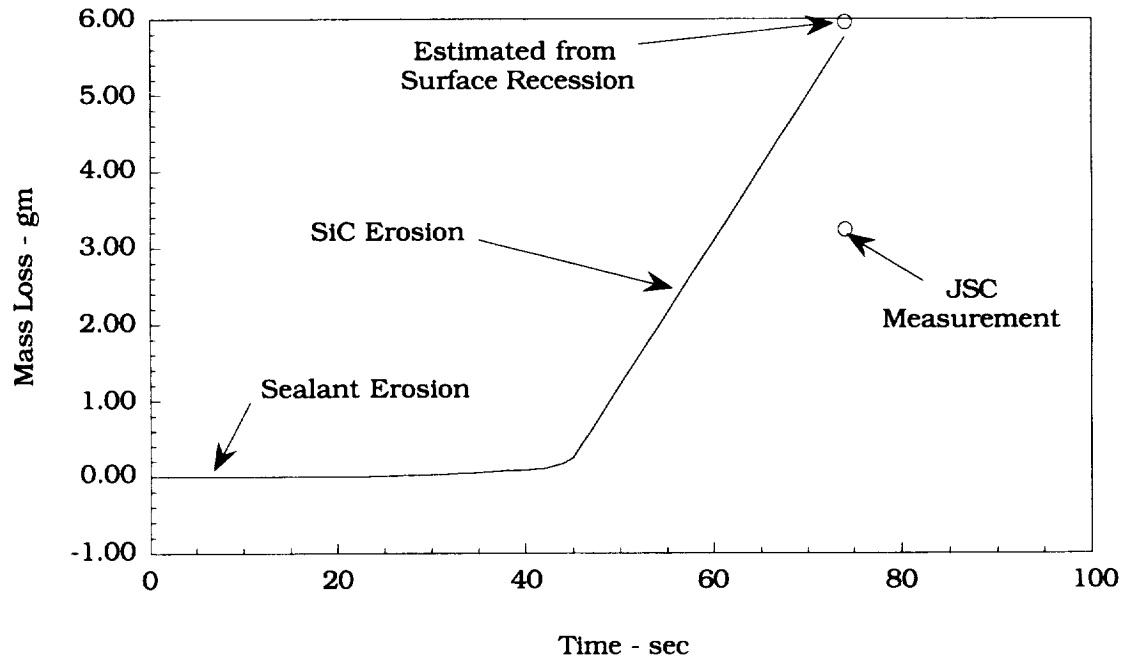

Fig. 13b Predicted Mass Loss History for IN-06.

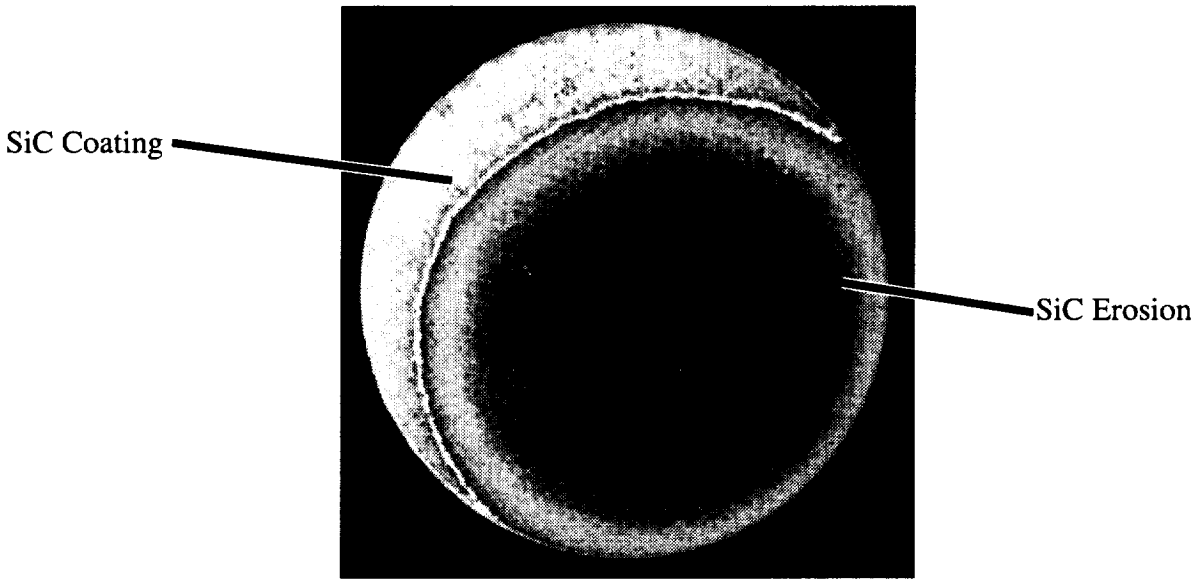

Fig. 14 IN-06 Surface Erosion (SiC Diffusion-Limited) Post-Test Photograph.

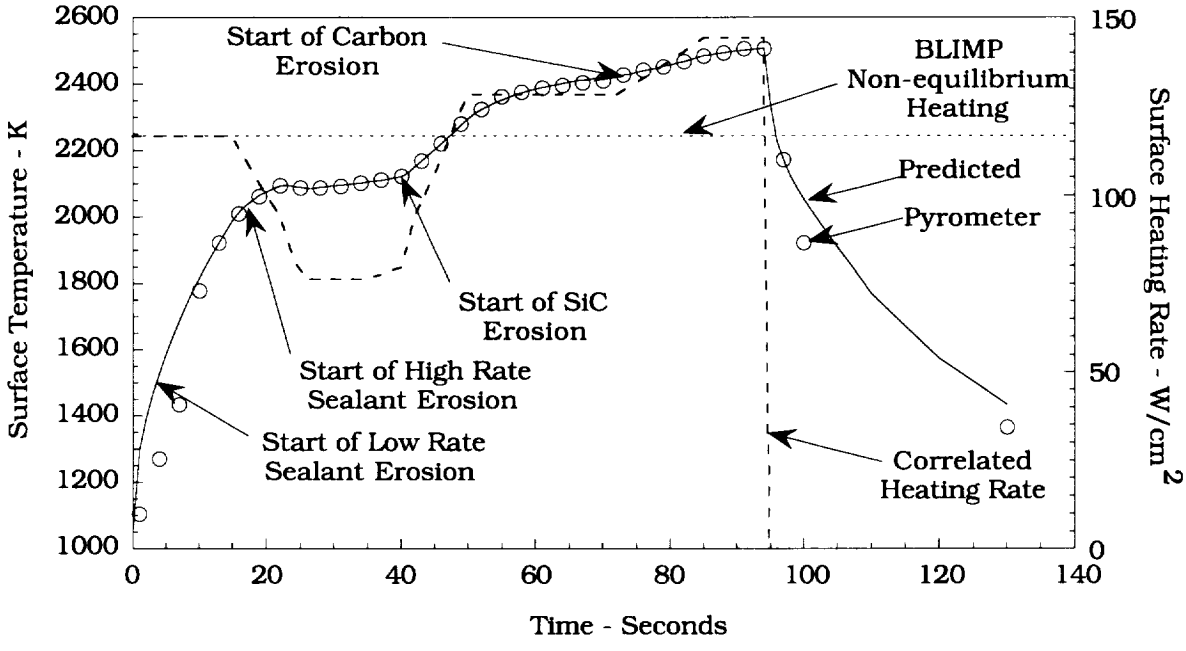

Fig. 15 Comparison Between Predicted and Experimental Surface Temperatures and Heating Rates for IN-20.

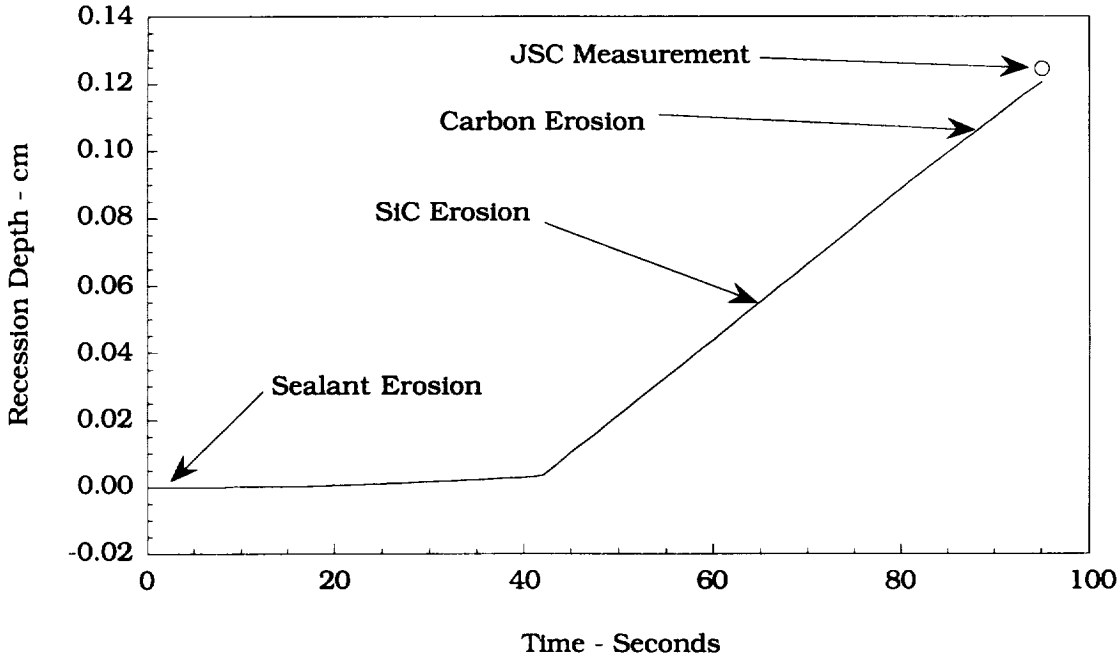

Fig. 16a Predicted Recession Depth Time History for IN-20.

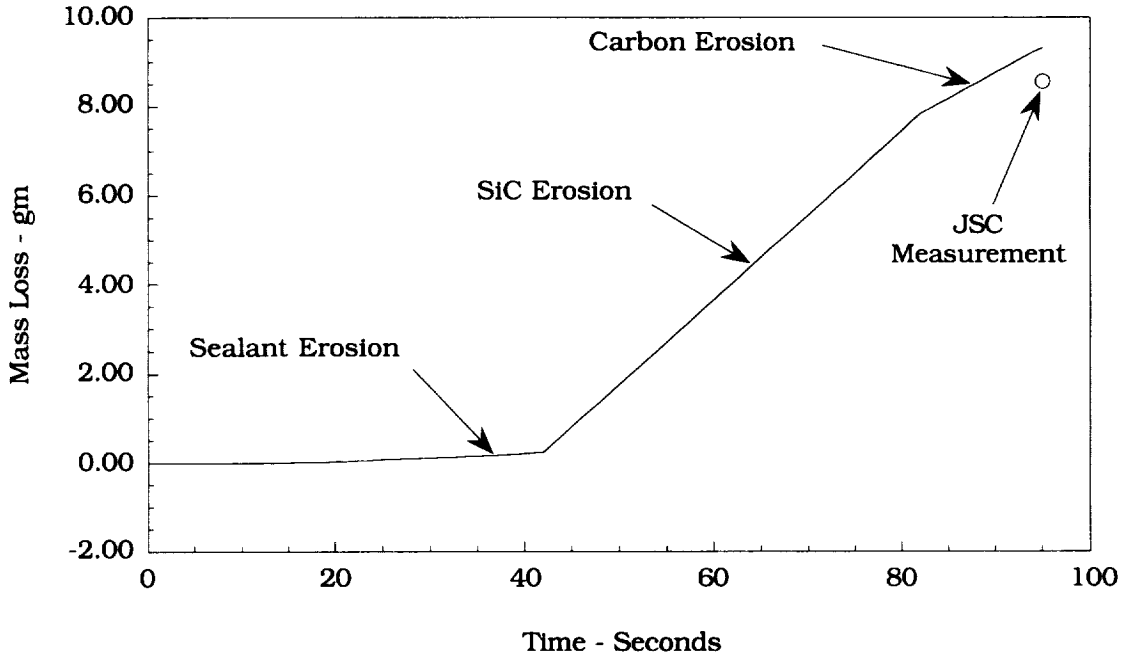

Fig. 16b Predicted Mass Loss History for IN-20.

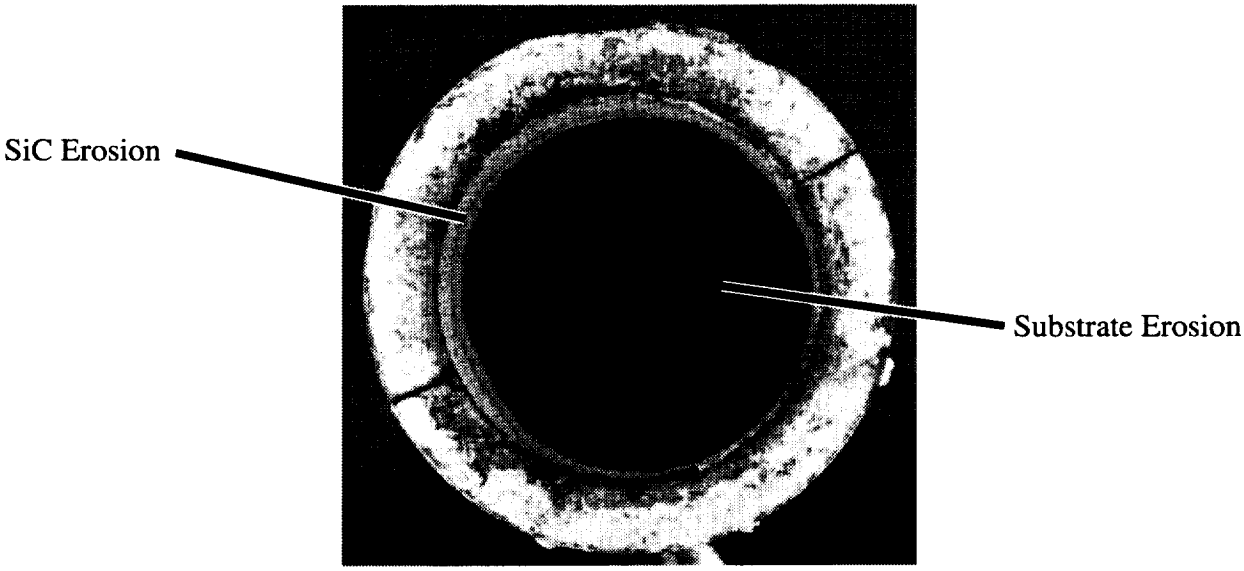

Fig. 17 IN-20 Surface Erosion Post-Test Showing Effects of Sealant/Coating/Substrate Erosion.

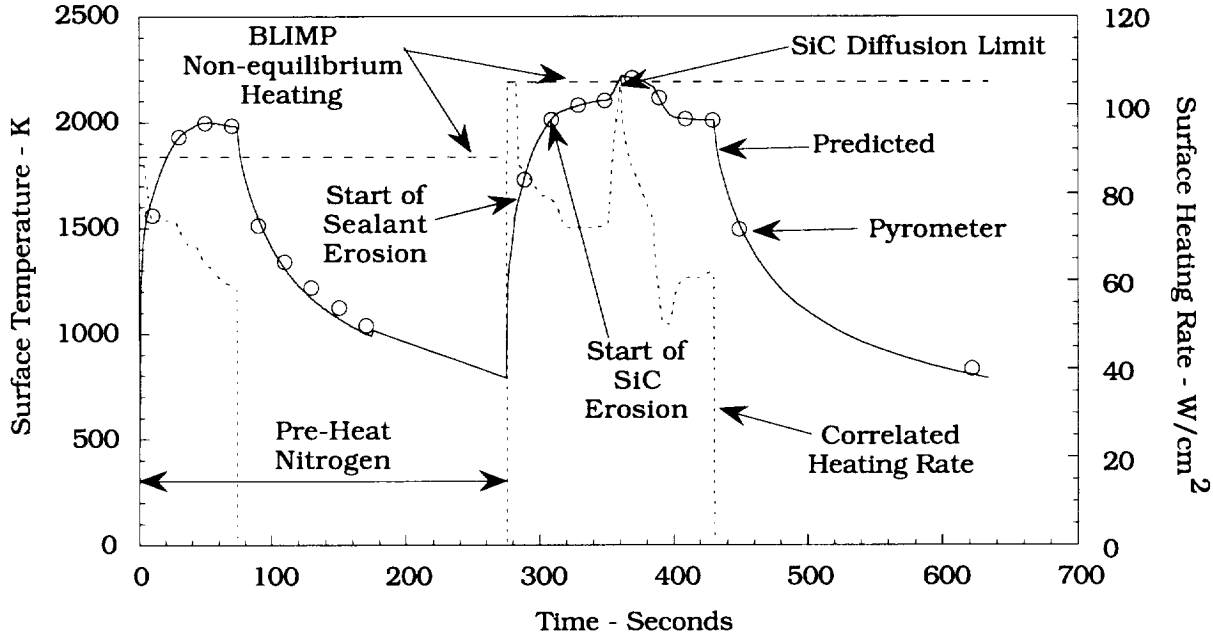

Fig. 18 Comparison Between Predicted and Experimental Surface Temperatures and Heating Rates for Abort Simulation for AU-05.

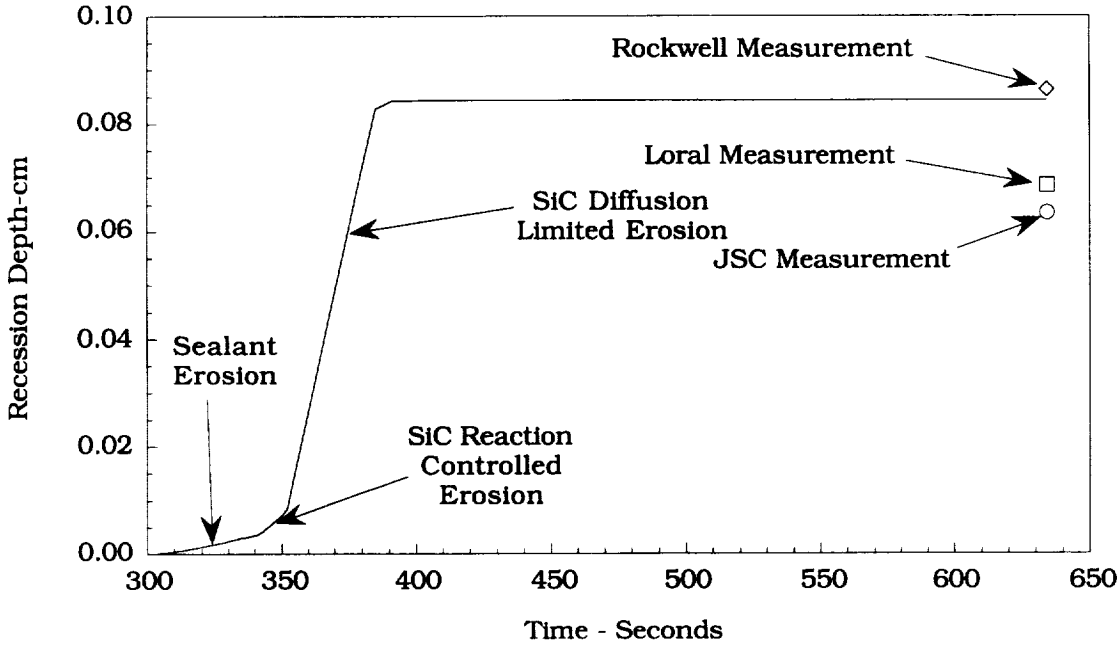

Fig. 19a Predicted Recession Depth Time History for the Abort Simulation for AU-05.

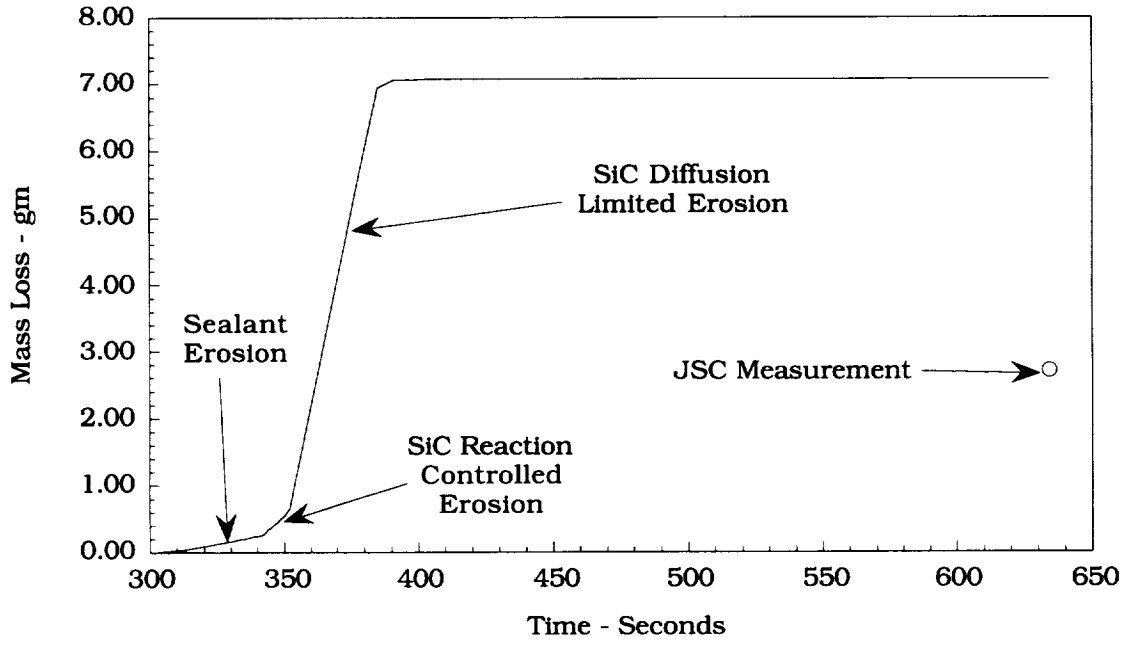

Fig. 19b Predicted Mass Loss History for the Abort Simulation for AU-05.

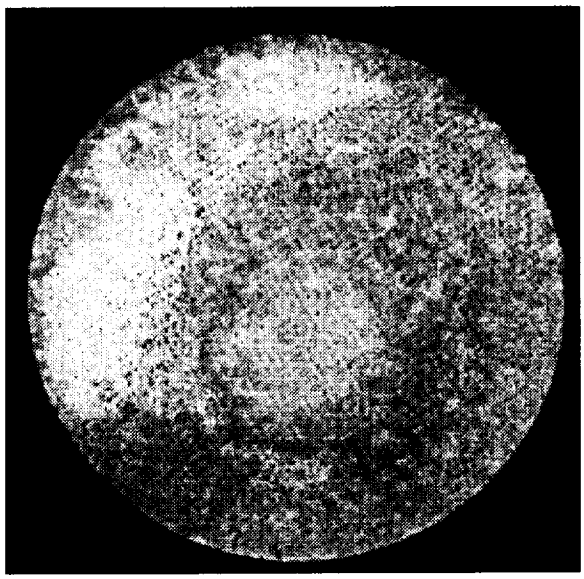

Fig. 20 Post-Test Photograph of Simulated Abort Test Condition for AU-05.

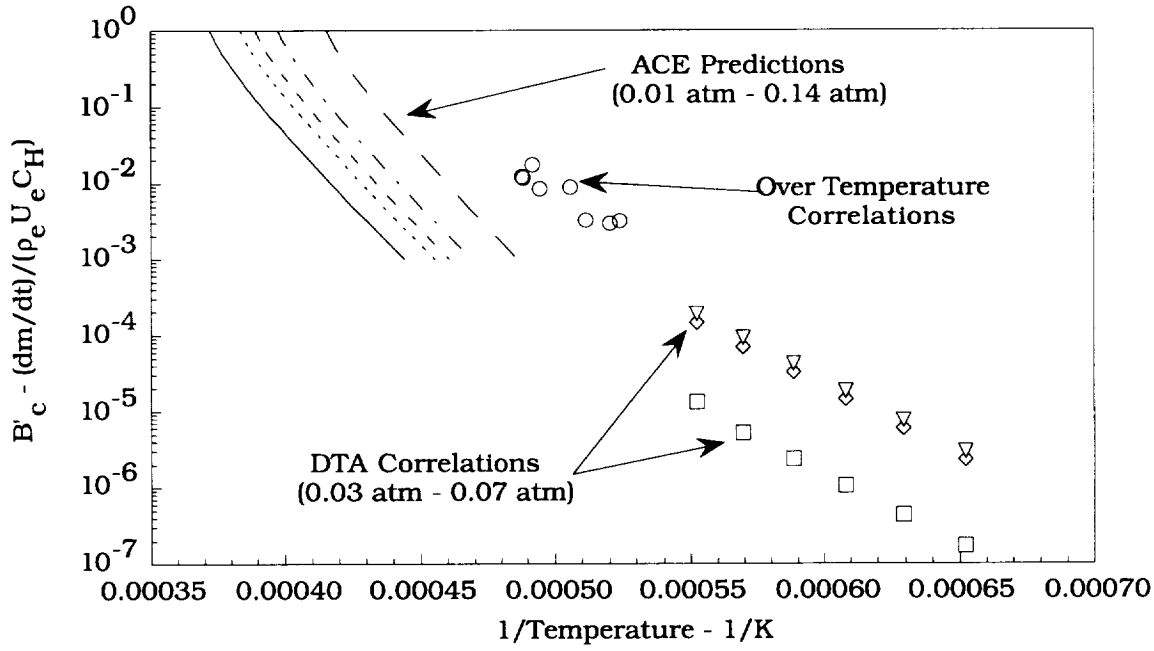

Fig. 21 Comparison of Na_2SiO_3 Ablation Rates Calculated by ACE and Sealant Correlations Using Arc-Jet Test Data.

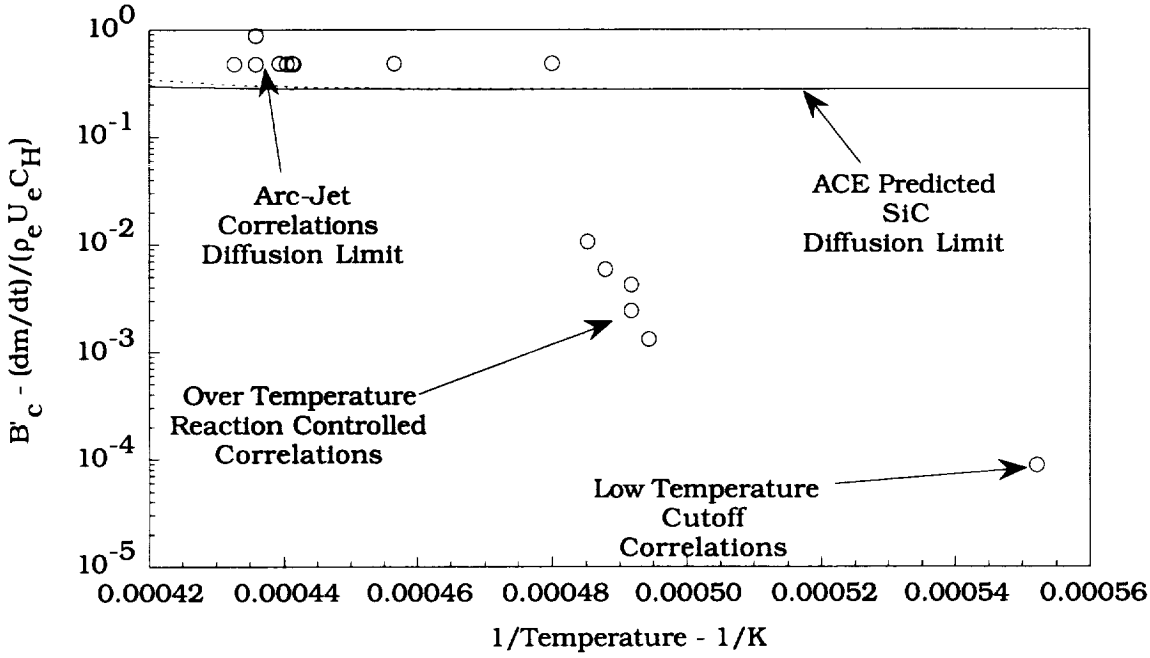

Fig. 22 Comparison of SiC Ablation Rates Calculated by ACE and SiC Coating Correlations Using Arc-Jet Test Data.

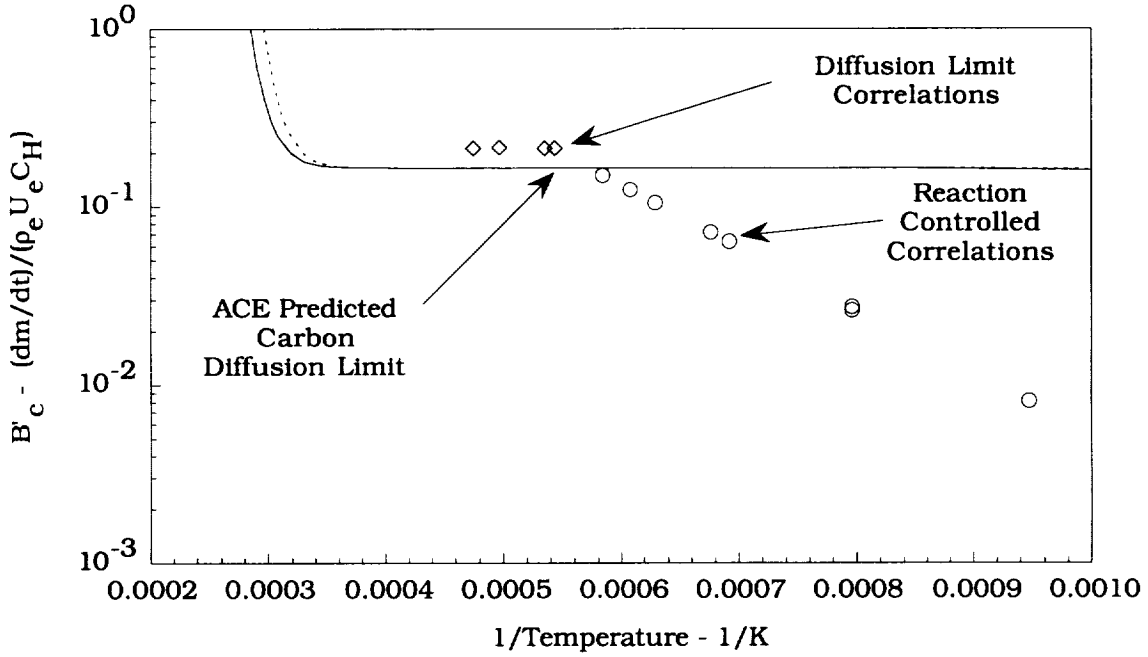

Fig. 23 Comparison of Carbon Ablation Rates Calculated by ACE and RCC Carbon Substrate Correlations Using Arc-Jet Test Data.

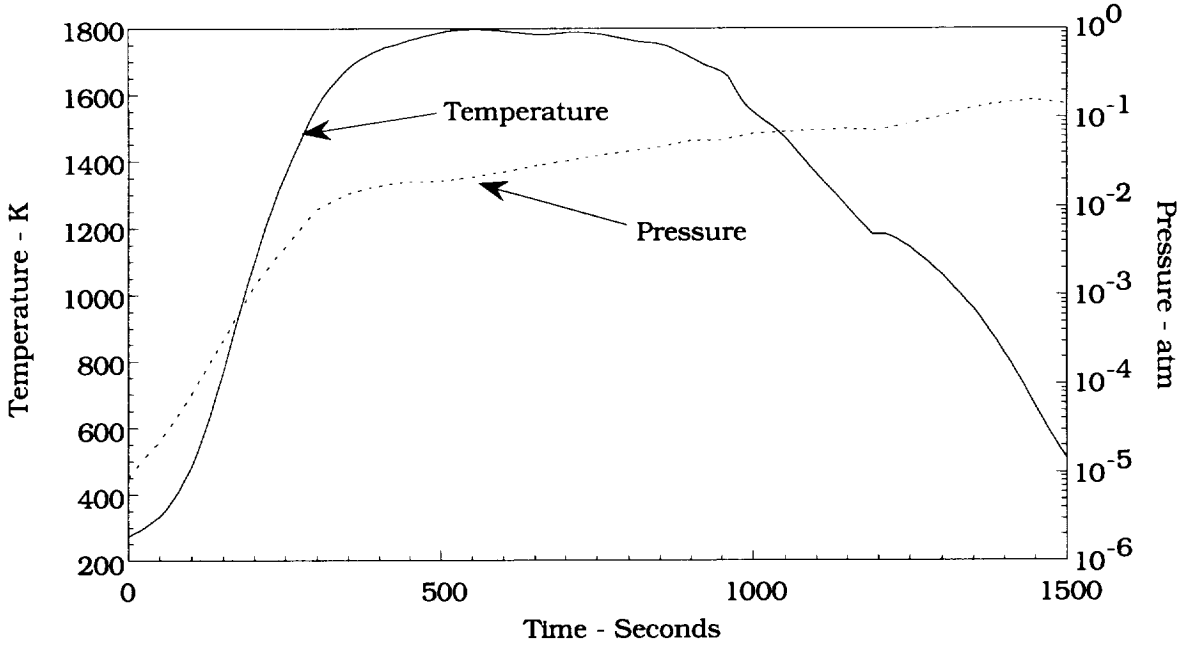

Fig. 24 Stagnation Point Surface Temperature and Pressure on the Wing Leading Edge Panel 9 for a Nominal Mission.

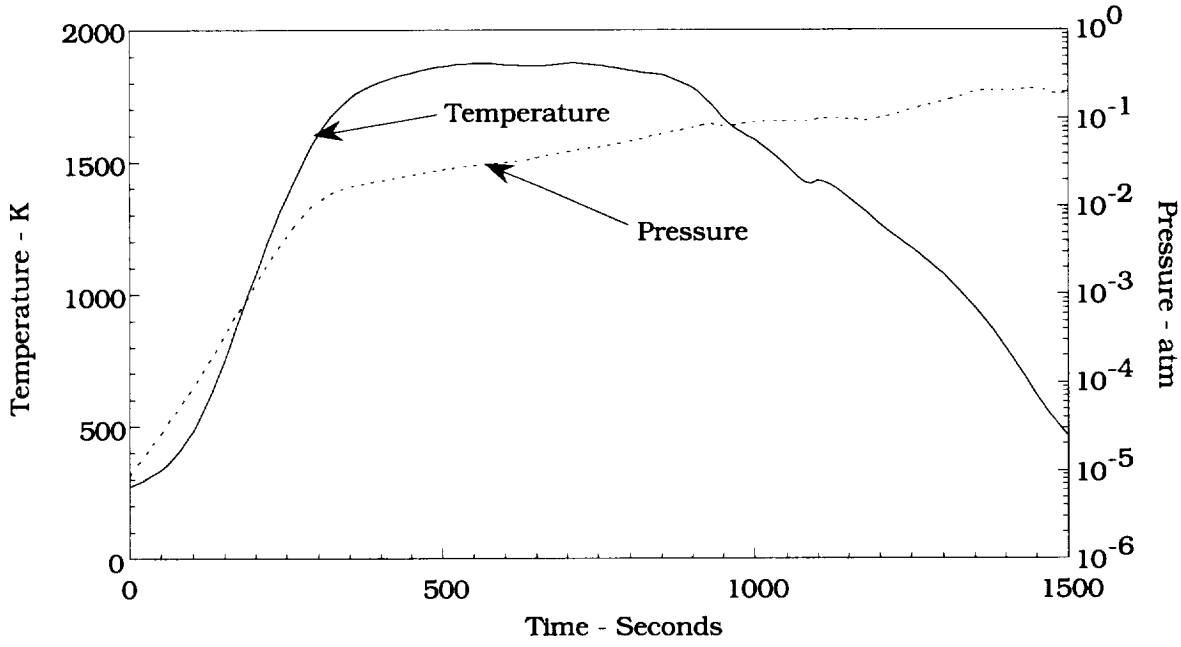

Fig. 25 Stagnation Point Surface Temperature and Pressure on the Wing Leading Edge Panel 9 for a Heavy Weight Mission.

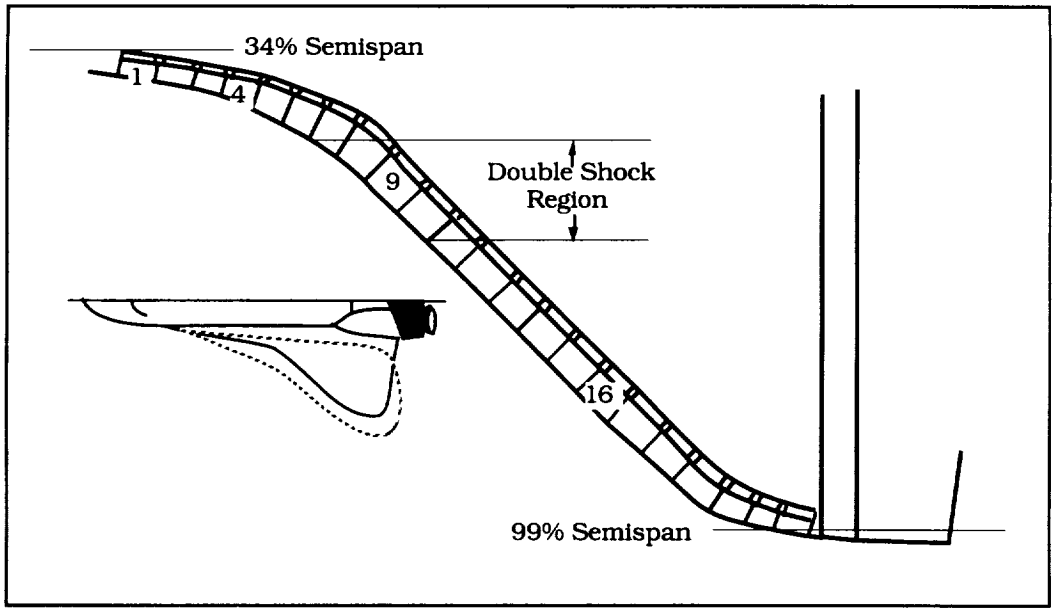

Fig. 26 Sketch of the Wing Leading Edge Panel Locations.

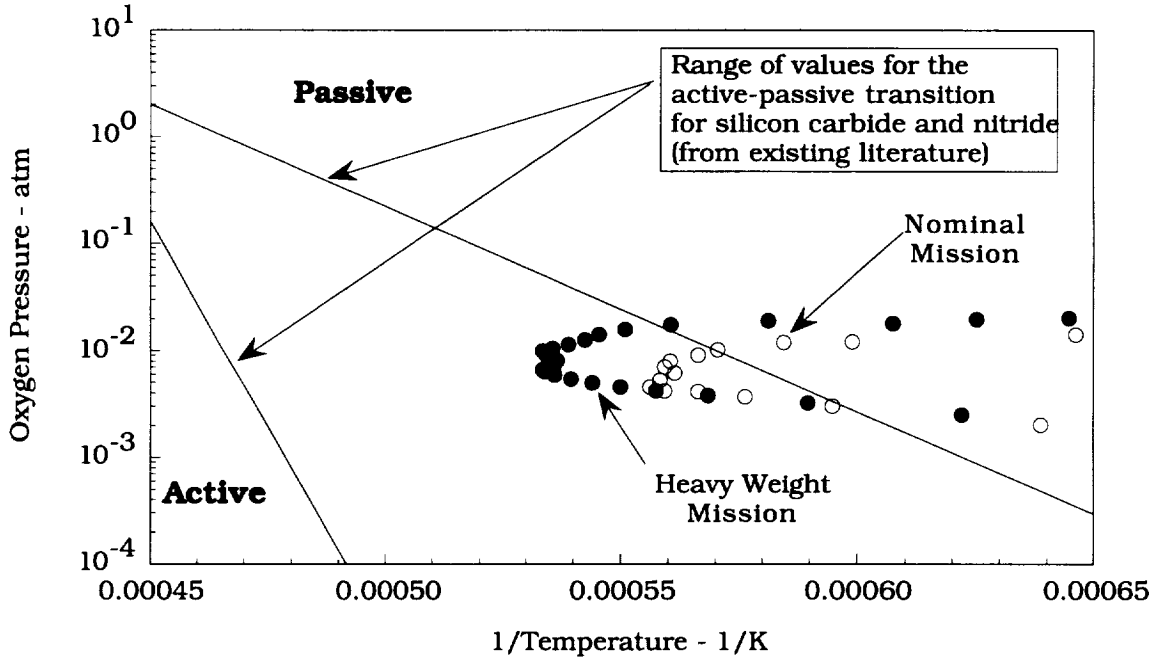

Fig. 27 Active-Passive Transition Oxygen Pressure Comparisons With Flight Conditions.

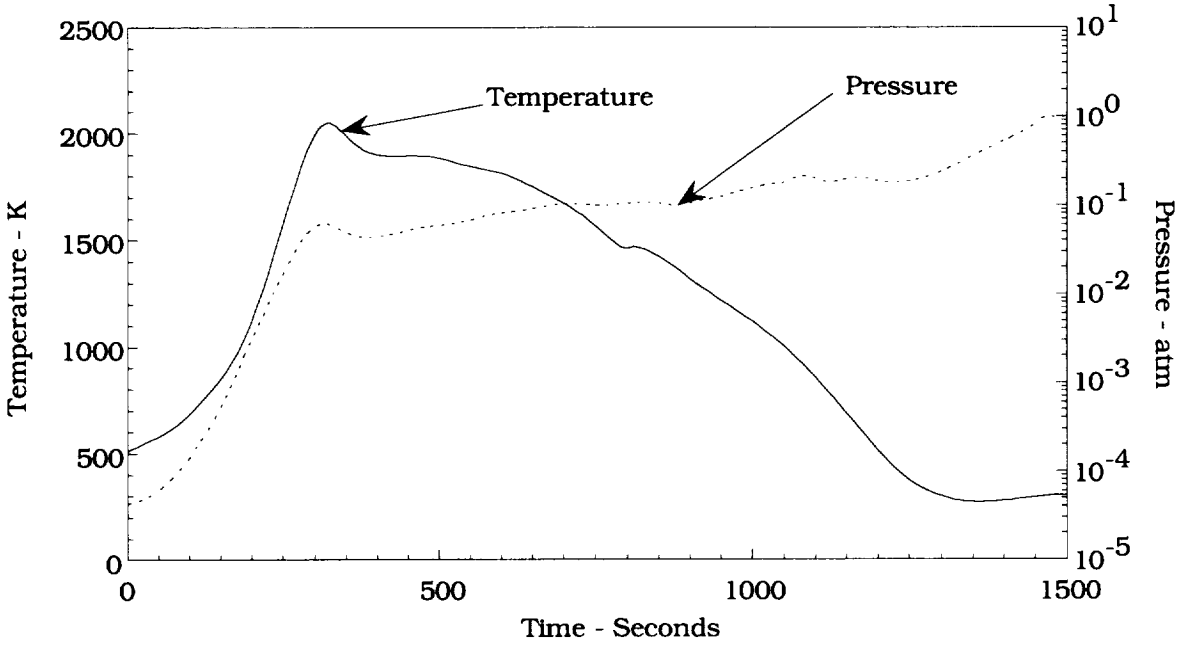

Fig. 28 Stagnation Point Surface Temperature and Pressure on the Wing Leading Edge Panel 9 for an Abort Mission.

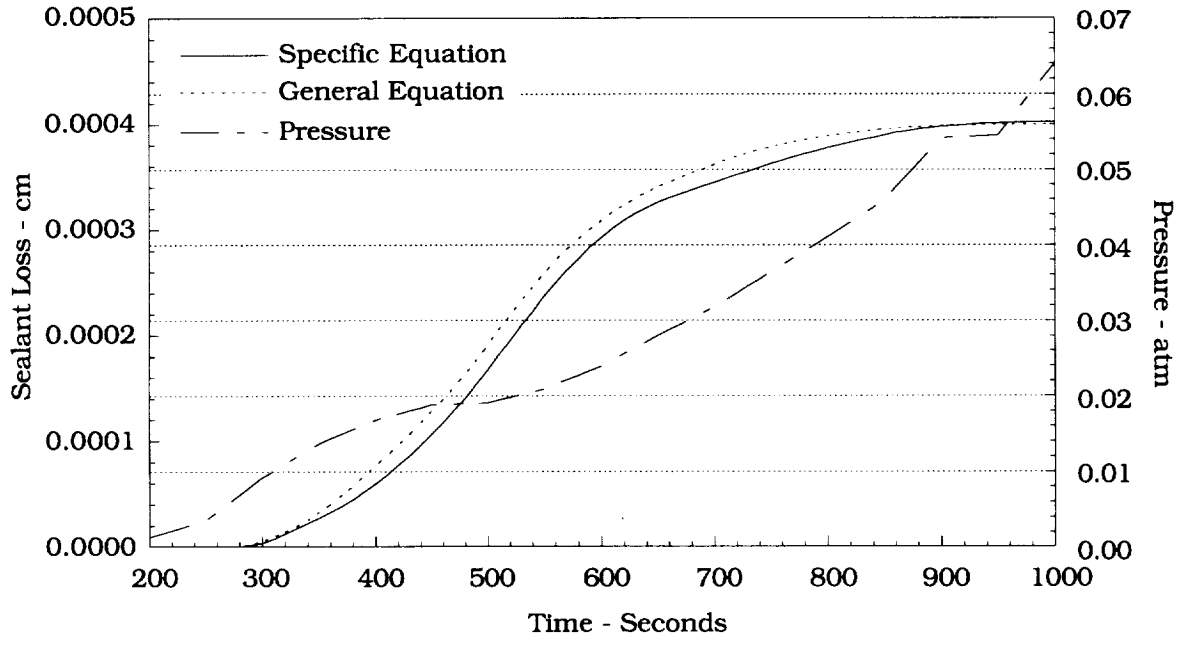

Fig. 29 Correlated Sealant Mass Loss and Pressure on the Wing Leading Edge Panel 9 for a Nominal Mission.

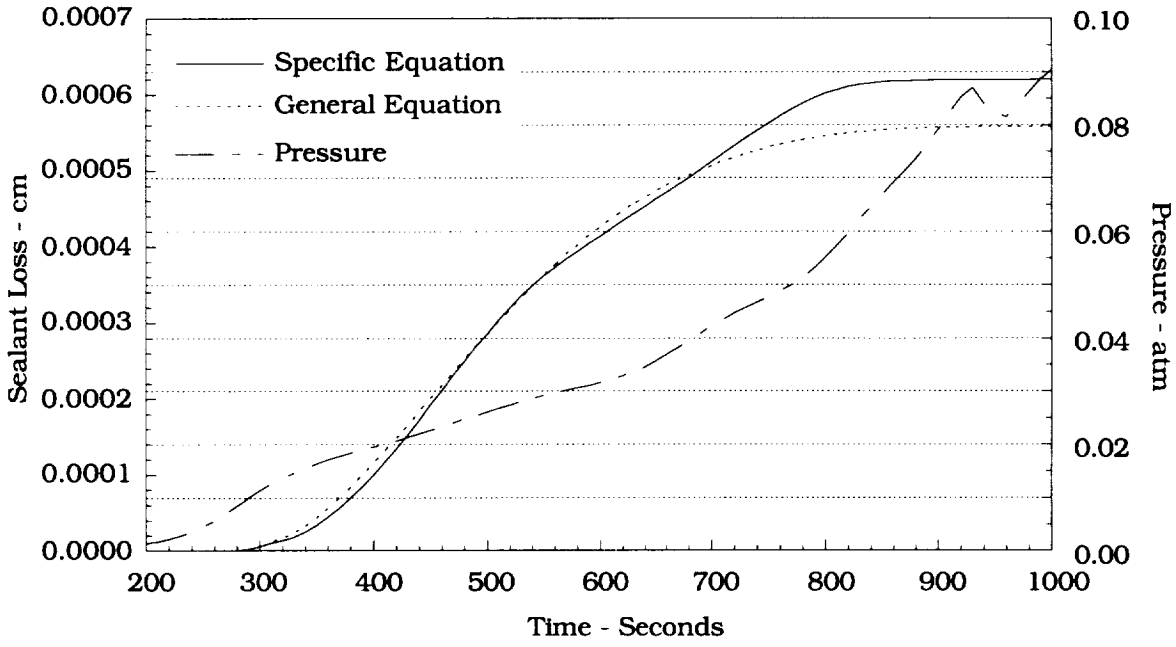

Fig. 30 Correlated Sealant Mass Loss and Pressure on the Wing Leading Edge Panel 9 for a Heavy Weight Mission.

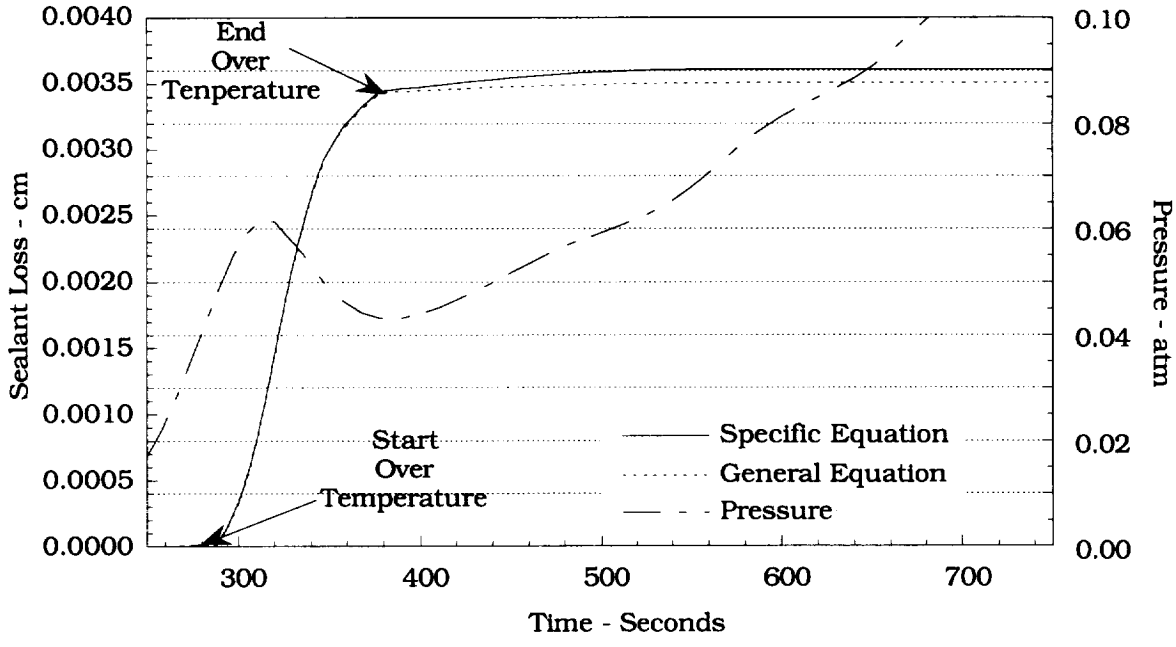

Fig. 31 Correlated Sealant Mass Loss and Pressure on the Wing Leading Edge Panel 9 for an Abort Mission.

Appendix A

Error Analysis

Appendix A - Error Analysis

Conceptually the error analysis should be simple and straightforward, but from a practical viewpoint the error analysis is just as complicated as the original analysis. Additionally, the DTA error analysis should be the simplest of all since the tests extend over hours, not just a few seconds, and small errors in time are minimized. Unfortunately, this is not true since the mass loss is very small and some tests indicate an increase in mass–not a loss. This analysis is based only on test data that resulted in mass loss or surface recession.

Calibration models were made to correlate surface temperatures measured with thermocouples with the laser pyrometer. Although there is a conduction heat loss through the thermocouple lead wires, thermal analysis from previous RCC test programs indicated that the actual surface temperature should not be more than 8.3°C (15°F) higher than the measured values. Previous analysis also indicated that the recorded laser pyrometer surface temperature is within 5% of the actual surface temperature. The laser pyrometer starts recording temperatures when the surface reaches approximately 810 K.

Sealant Error Analysis

DTA Sealant Error Analysis

The basic test data for the DTA sealant mass loss is summarized in table I in the main text. These tests were conducted at the constant temperature and pressure levels indicated. For analysis purposes it is more desirable to control the surface temperature instead of the heating rate since temperature is one of the characterizing parameters used in the sealant correlations. In general, two test articles were prepared and tested for each test condition. Under ideal conditions there would be minimal data scatter. This did not always occur as there is some evidence of data scatter. This will be addressed in more detail later.

It is assumed that the sealant mass loss on the cylindrical test articles occurred only on the flat surface face exposed to the heated Arc-Jet plasma. It is further assumed that temperature and pressure variations were minimal and that the sealant was uniformly distributed on each test article's surface.

The basic mathematical assumption is that the sealant loss rate follows an Arrhenius formulation as given by Eq. (A-1)

$$\dot{m} = k\left(p / p_0\right)^n e^{-E/RT} \tag{A-1}$$

where $\dot{m}$ is the mass loss rate per unit area, k is the pre-exponential coefficient in the same units as $\dot{m}$, E/R and T are units of temperature, p is the stagnation pressure, and p_0 is the reference pressure at 1 atm in the same units as p. This implies that the mass loss rate data will fall on some straight line when plotted on a semi-log plot vs. the inverse of temperature. The mathematical effort is to obtain the curve fit that minimizes the error between the prediction and the observed data. A second assumption is that the data for any given pressure may be isolated for purposes of curve fitting. This simplifies the analysis since pressure is removed as a variable for each set of data. Of course, pressure must be reintroduced into the formulation after all data has been analyzed. In this error analysis discussion, when reference is made to Eq. (A-1) in its full form it will be referred to as the "general equation," but when the exponent for pressure is zero, n=0, it will be referred to as the "specific equation."

Early in this program it was obvious that the number of samples available for measurement and analysis was limited. A decision was made to compute the average mass loss rate (lb/ft^2 -hr or gm/cm^2 -hr) as a basis of analysis and predictions. If the mass for a specimen increased at the end of the test period, it was no longer considered in the data reduction process and the data for the remaining specimen was used. For all practical purposes only data for the 0.07-atm, 0.05-atm, and 0.03-atm test conditions can be used for curve fitting. All other curve fits must be derived from this analysis due to the limited number of data values available. Initial analysis involved the average mass loss rate data on an inverse temperature plot and assessing predicted curve fits to the data. Data from the 0.01-atm tests were used only to emphasize the pressure-dependent nature of the data and initially the 0.014-atm data were not available. From this

preliminary data analysis it became clear that, in general, the 0.05-atm and 0.03-atm data were essentially indistinguishable while data taken at other pressures (0.07 atm and 0.01 atm) were quite distinct. The slope of the 0.07-atm data was in close agreement with the slopes of the 0.05-atm and 0.03-atm data. The 0.05-atm and 0.03-atm data were combined into a blind data set (no identification with respect to their origin was maintained) and far outlying data was eliminated from the correlating fit.

The resulting correlated curve fit, using the specific equation, was obtained with a residual accuracy of 99.38% (a residual accuracy of 100% implies an exact fit through every measured data point). A comparison of the correlated curve fit data to all of the average measured data values can be seen in figure A-1. This is an excellent fitting of the data even though some of the outlying data appears to be far removed from the regression line. The corresponding variation of the percent error ranged from +6% to +10% for the 0.05-atm data and -22% to +12% for the 0.03-atm data. Outlying data had errors in excess of ±100%. A comparison with all data (using the specific equation) can be seen in figure A-2. Variations for all data values from the correlated regression line follow the same trend as for the averaged data values, but are slightly greater in magnitude, see table A-1 for actual data values.

Data correlation (using the specific equation) for the 0.07-atm data was achieved using the same exponential factor, -E/R, obtained for the 0.05-atm and 0.03-atm data. As before, any outlying data was ignored for regression analysis. The resulting correlated curve fit was within 20% of the average measured data values (fig. A-3 and table A-2). This data is in excellent agreement with the regression line. Observe that the slope is consistent with the data which implies that a general correlation in the form postulated by Eq. (A-1) can be made. If the outlying data at 1756 K are ignored when comparisons are made with all data, similar excellent results are obtained (fig. A-4).

Data correlation for the 0.014-atm and 0.01-atm data (using the specific equation) was obtained in a similar manner with little difficulty since only minimal data existed for these tests. Tabulated values of the variations are shown in table A-2 along with the 0.07-atm data. Corresponding plots showing the correlated regression lines with average and all mass loss rate data at these pressures can be seen in figures A-5 and A-6, respectively. Only the data for the 0.01-atm tests show any appreciable scatter.

An interesting comparison can be seen in figures A-7 and A-8 where ±50% error bands have been placed on the data curves (specific equation) for the 0.05/0.03 atm and 0.07 atm data, respectively. These plots illustrate the degree of scatter in the (nonnegative) data that is not intuitively obvious in the previous plots. This illustrates that the ±50% error bands are quite close to the regression line on the scale used for these plots and further illustrates the scatter associated in the outlying data.

The general equation, Eq. (A-1), correlating all data as a function of both temperature and pressure, is illustrated in figure A-9. In general, this representation of the data set is conservative in predicting the mass loss rate except for the 0.01 atm data, although the representation for the 0.05 atm data appears to be more closely associated with the outlying data than the data used for correlation. The correlation with respect to the different coefficients as a function of pressure can be seen in figure A-10. This represents the product $k\left(p / p_0\right)^n$ in the general equation (A-1). It is also observed that the coefficient for the 0.05-atm data is poorly represented by this approximation. This implies that the greatest error will occur in some pressure range surrounding 0.05 atm when using the general equation.

Of somewhat more interest is consideration of error bands about the general equations regression line with respect to the measured mass loss rate. In figure A-11 a -75% error band is used to compare with the regression line for the 0.07-atm data. As can be seen in this figure, the -75% error band and the regression line shown bound the majority of the data. Similar results are obtained when comparing the +150% error band for the 0.05-atm data, and the -25% error band for the 0.03-atm data (figs. A-12 and A-13). Correlation error bands of -40% were used for the 0.014-atm data and bound all four data values (fig. A-14). Correlation error bands of +30% and -40% for the 0.01-atm data are shown in figure A-15. These error bands bound both data values.

These results are not in as close agreement as the single pressure regression curves developed from the averaged data, but can be used in estimating the corresponding error in prediction of sealant loss in flight. The greatest error occurs for the 0.05-atm data as would be expected from examining figure A-10, where errors in predicting the coefficient were greater at the higher pressures (0.05 atm and 0.07 atm).

Over-Temperature Sealant Error Analysis

The basic test data for the over-temperature sealant mass loss is summarized in table IIIa in the main text. Fourteen test articles were used in this analysis. At these higher heating conditions the sealant loss data were not pressure dependent, which effectively sets n = 0 in Eq. (A-1) (see earlier comments with respect to the specific equation). The analysis for this data differed from the DTA analysis in that the recession depth was used instead of mass loss for calculating the mass loss rate. At this higher heating, the sealant loss was not uniformly distributed over the heated surface. Additionally, beads of SiO_2 formed on the surface and were observed after the test was complete. Thus, the measurements were in effect based on depth probes and knowledge of the sealant density and exposed surface area. The resulting correlated curve fit to the averaged data was obtained with a residual accuracy of 94.36%. A comparison of the correlated curve fit data to the average measured data can be seen in figure A-16. This illustrates a reasonable agreement with the data. A comparison of the regression line with all over-temperature data with ±35% error bands can be seen in figure A-17. These error bands encompass a majority of the data, although there are some outlying data points. These results using the specific equation are in relatively close agreement to the averaged data, and can be used with a high degree of confidence in obtaining conservative estimates of sealant loss in flight.

SiC Coating Error Analysis

The basic test data for the SiC coating mass loss is summarized in table IIIb in the main text. SiC ablation analysis is based on the natural progression of the sealant analysis. For instance, before any coating ablation, the protective sealant must be eroded, exposing the SiC coating to the heated oxidizing gases. From the DTA analysis it was observed that the sealant mass loss rates were low, and could be ignored for the SiC coating analysis. However, the over-temperature sealant mass loss must be included to correctly assess the SiC erosion characteristics.

The test articles were inserted into the Arc-Jet heated plasma and, as with the sealant tests, an attempt was made to expose the models such that a constant temperature would be maintained on the surface. In practice, this goal was achieved as long as the sealant remained on the surface.

These tests can be subdivided into three regions based on surface temperature and analysis: low-temperature (1811 K to 1967 K), rate-controlled (1967 K to 2136 K), and diffusion-limited (2136 K to 2478 K).

SiC Coating Diffusion-Limited Error Analysis

This analysis was aided by an observed "hot spot" that developed on the surface of the specimen. Hot spot refers to a rapid increase in temperature at approximately 2061 K on the surface of the model which is an observable transition at pressure below 0.095 atm, but the transition becomes less distinct at higher pressure. The onset of the hot spot can be identified in real time on the facility video monitor or graphically from the surface temperature time history. Due to the orientation of the laser pyrometer, the time the "hot spot" was recorded was approximately one second later than that recorded by engineers observing the test. Five basic assumptions are made in this analysis:

- Sealant erosion can be ignored below 1922 K
- Over-temperature sealant erosion would continue until the commencement of SiC coating erosion
- Over-temperature sealant erosion occurred at a constant temperature
- SiC coating erosion did not start until one second before the "hot spot" developed
- SiC coating erosion occurred at the median temperature between the start of SiC erosion and the end of SiC erosion

Nine test articles were used in this analysis, and carbon substrate erosion was observed on four specimens. On one specimen, IN-12, the hot spot was not a true indication of SiC ablation, and an assumed sealant thickness of 0.0762 mm was used in the analysis. All other sealant thicknesses were computed based on the over-temperature sealant mass loss rates. As with the sealant test data, average data values were used for regression analysis. Initial analysis attempts were made assuming the Arrhenius form shown in Eq. (A-1), but it soon became obvious that this data was different. The resulting correlation curve compared to the average mass loss data can be seen in figure A-18. In this figure the correlated data curve is presented covering the temperature range from 2136 K to 2478 K. A comparison of the

regression line with all diffusion-limited data with ±10% error bands can be seen in figure A-19. The outlying data point at 2083 K represents uncertainty in the rate-controlled data, as will be discussed later. As can be seen in these figures the diffusion-limited data is known quite well. These results using the specific equation (k=17.123 gm/cm^2 -hr) are in excellent agreement to the regression line calculated for the averaged data, and can be used with utmost confidence in obtaining conservative estimates of SiC coating loss in flight.

SiC Coating Rate-Controlled Error Analysis

Six test articles were used in this analysis, and no carbon substrate erosion was observed on any specimen. The data appears to be divided into two distinct bands of data: high-rate and low-rate. All data sources for the low-rate data indicated a decrease in thickness, while some sources for the high-rate data indicated an increase in thickness. Separate correlations, assuming the Arrhenius form, were made for both the high-rate and low-rate data. Regression analysis accuracy was 99.8 % for the low-range data and 97.9% for the high-range data. The percent error range for these two curve fits was -2.8% to 4.8% for the low-range data and -19.0% to 8.9% for the high-range data. The slope, E/R, for the low-range data was selected for use for the general correlation of these data. The results of this correlated analysis can be seen in figure A-20. In this figure, error bands of +90% and -50% are shown to represent data uncertainty. From this figure it can be seen that all of the data is encompassed, and more accuracy is given to the low-rate data than to the high-rate data. On the semi-log plot the regression appears to evenly divide the two sets of data. These results using the specific equation are in relatively close agreement to the measured data, and can be used with confidence in obtaining conservative estimates of SiC coating loss in flight.

SiC Coating Low-Temperature Error Analysis

Only two specimens from previous tests were used to determine the SiC low temperature cut-off limit. These two tests were conducted at a constant temperature of 1811 K and pressure of 0.05 atm for 8 hours. As opposed to the other SiC coating tests, no eddy current data were available for estimating the coating thickness. Likewise, at these low temperatures, no hot spot developed to aid as an indicator for the initiation of SiC coating erosion. Additionally, no test data plots were available for analysis.

Analysis was performed assuming three sealant thickness values: a minimum of 0.0127 mm, a mid range of 0.0254 mm, and a maximum of 0.0381 mm. It was assumed that both specimens had the same amount of sealant. The minimum value was selected for use to provide a conservative estimate for SiC coating erosion. The regression fit for the 0.05 atm DTA sealant mass loss rate was used for sealant mass loss calculations. The results of this correlated analysis can be seen in figure A-21. In this figure error bands of ±20% are shown to represent data uncertainty. From this figure it can be seen that these error bands encompass all of the data. The low-temperature data is known only at one temperature (1811 K). However, the results using the specific equation (k=1.846 x 10^{-3} gm/cm^2 -hr) are in excellent agreement with the averaged data, and can be used with confidence in obtaining conservative estimates of SiC coating loss in flight at the low-temperature range.

RCC Carbon Substrate Error Analysis

The basic test data for the RCC carbon substrate mass loss is summarized in table IIIc in the main text. From the previous work of Scala[14] there was an indication that the carbon substrate mass loss rate could be correlated as a function of the pressure to the ½ power. A successful correlation effort was achieved when it was recognized that the data were not one continuous curve, but consisted of two components: a diffusion-limited component (similar to ACE predictions), and a rate-controlled component (similar to Scala predictions). Due to the limited data available, no data averaging was used in this analysis.

RCC Carbon Substrate Diffusion-Limited Error Analysis

Six specimens were used in the carbon substrate diffusion limit analysis. These data were taken over a temperature range from 1840 K to 2145 K and a pressure range from 0.028 atm to 0.147 atm. Initial

correlation efforts lead to very large E/R values which indicated that $e^{-E/RT} \approx 1$. The regression line derived from this data along with ±10% error bands can be seen in figure A-22. As can be seen, this provides an excellent correlation of the data and can be used with utmost confidence at temperatures well above 2145 K.

RCC Carbon Substrate Rate-Controlled Error Analysis

Ten specimens were used in the carbon substrate rate-controlled analysis, two of which (at 1838 K and 1867 K) were also used in the diffusion-limited analysis. These data were taken over a temperature range from 1056 K to 1867 K and a pressure range from 0.028 atm to 0.142 atm. Regression accuracy was 94.7% for this data. The regression line derived from these data along with ±20% error bands can be seen in figure A-23. As can be seen, this provides an excellent correlation of the data and can be used with confidence at temperatures in the 1056 K to 1867 K range.

Table A-1. DTA Percent Error Variations at Pressures of 0.05 atm and 0.03 atm for Predicted and Measured Data

Specimen	Pressure atm	Temperature K	Measured mdot/area gm/cm^2-hr	Average Measured mdot/area gm/cm^2-hr	%Error Average to Measured	Predicted mdot/area gm/cm^2-hr	%Error Predicted to Measured	%Error Predicted to Average Measured
1B15	0.050	1922	1.04727E-02	1.06116E-02	1.33	1.13934E-02	8.79	7.37
2B15		1922	1.07506E-02		-1.29	1.13934E-02	5.98	
1A23		1811	1.76574E-03	2.76519E-03	56.60	3.03745E-03	72.02	9.85
2A23		1811	3.76464E-03		-26.55	3.03745E-03	-19.32	
1A21		1756	5.48299E-04	6.58101E-04	20.03	1.47294E-03	168.64	123.82
2A21		1756	7.67903E-04		-14.30	1.47294E-03	91.81	
1A19		1700	2.64052E-04	2.59755E-04	-1.63	6.81262E-04	158.00	162.27
2A19		1700	2.55457E-04		1.68	6.81262E-04	166.68	
1A17		1644	2.43515E-04	2.81856E-04	15.74	2.99101E-04	22.83	6.12
2A17		1644	3.20196E-04		-11.97	2.99101E-04	-6.59	
1A15		1533	-3.97349E-05		-661.70	4.82068E-05	-221.32	
2A15		1533	2.23192E-04	2.23192E-04	0.00	4.82068E-05	-78.40	-78.40
1B22	0.030	1811	4.09438E-03	3.91257E-03	-4.44	3.03745E-03	-25.81	-22.37
2B22		1811	3.73076E-03		4.87	3.03745E-03	-18.58	
1A22		1756	1.34391E-03	1.31405E-03	-2.22	1.47294E-03	9.60	12.09
2B20		1756	1.28418E-03		2.33	1.47294E-03	14.70	
1B18		1700	6.34175E-04	6.40163E-04	0.94	6.81262E-04	7.42	6.42
2B18		1700	6.46151E-04		-0.93	6.81262E-04	5.43	
1B16		1644	4.35218E-05	5.44255E-05	25.05	2.99101E-04	587.24	449.56
2B16		1644	6.53291E-05		-16.69	2.99101E-04	357.84	
1B14		1533	-3.42687E-05		-245.35	4.82068E-05	-240.67	
2B14		1533	4.98099E-05	4.98099E-05	0.00	4.82068E-05	-3.22	-3.22

Table A-2. DTA Percent Error Variations at Pressures of 0.07 atm, 0.014 atm, and 0.01 atm for Predicted and Measured Data

Specimen	Pressure atm	Temperature K	Measured mdot/area gm/cm^2-hr	Average Measured mdot/area gm/cm^2-hr	%Error Average to Measured	Predicted mdot/area gm/cm^2-hr	%Error Predicted to Measured	%Error Predicted to Average Measured
1B23	0.070	1811	3.10870E-04	2.62990E-04	-15.40	2.63766E-04	-15.15	0.29
2B23		1811	2.15111E-04		22.26	2.63766E-04	22.62	
1B21		1756	9.94784E-06	2.99498E-05	201.07	1.27907E-04	1185.77	327.07
2B21		1756	4.99518E-05		-40.04	1.27907E-04	156.06	
1B19		1700	3.42200E-05	4.97978E-05	45.52	5.91593E-05	72.88	18.80
2B19		1700	6.53755E-05		-23.83	5.91593E-05	-9.51	
1B17		1644	2.16685E-05	2.47937E-05	14.42	2.59733E-05	19.87	4.76
2B17		1644	2.79188E-05		-11.19	2.59733E-05	-6.97	
1A18	0.014	1700	3.34499E-03	3.12004E-03	-6.72	3.41692E-03	2.15	9.52
2A18		1700	2.89510E-03		7.77	3.41692E-03	18.02	
1A16		1644	1.60376E-03	1.65791E-03	3.38	1.50016E-03	-6.46	-9.52
2A16		1644	1.71207E-03		-3.16	1.50016E-03	-12.38	
1A14	0.010	1533	5.24121E-04	8.34061E-04	59.14	8.34061E-04	59.14	0.00
2A14		1533	1.14400E-03		-27.09	8.34061E-04	-27.09	

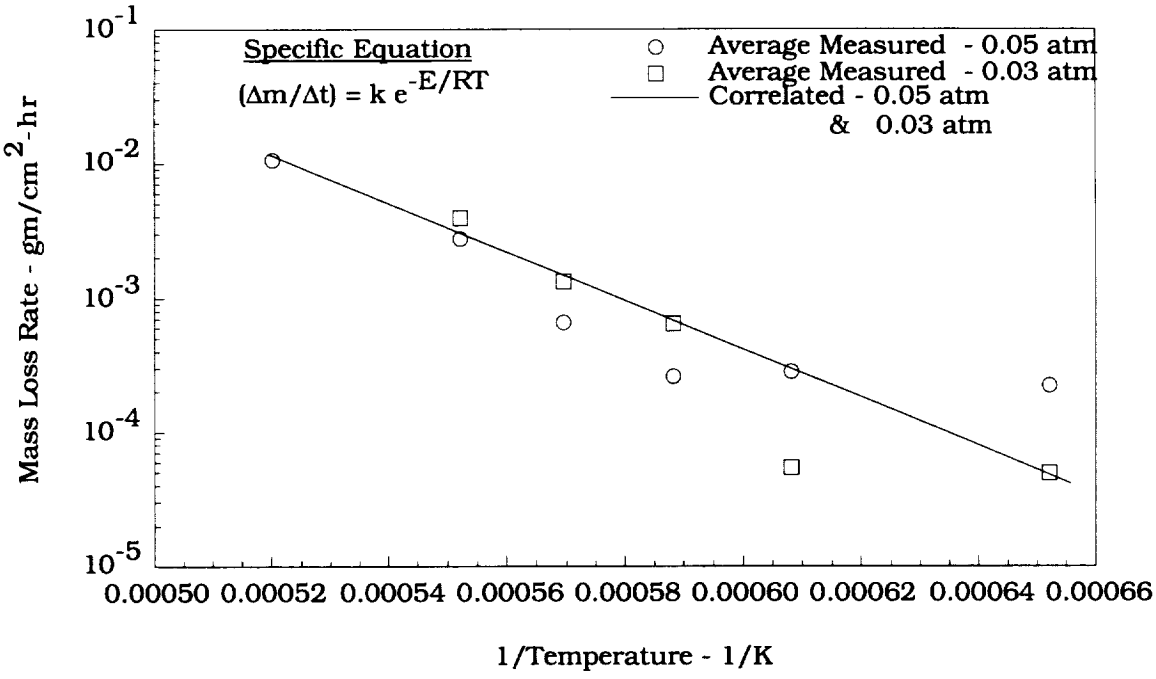

Fig. A-1 Comparison of the Correlated and Average Measured Mass Loss Rate for 0.05-atm and 0.03-atm DTA Sealant Data.

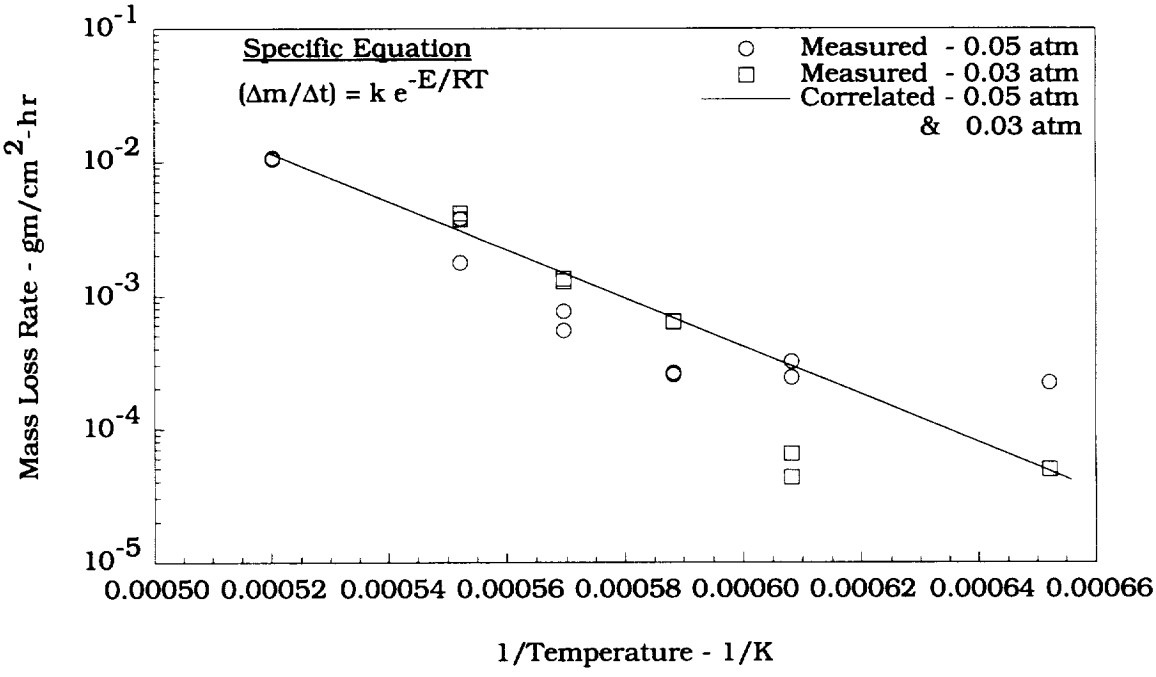

Fig. A-2 Comparison of the Correlated and Measured Mass Loss Rate for 0.05-atm and 0.03-atm DTA Sealant Data.

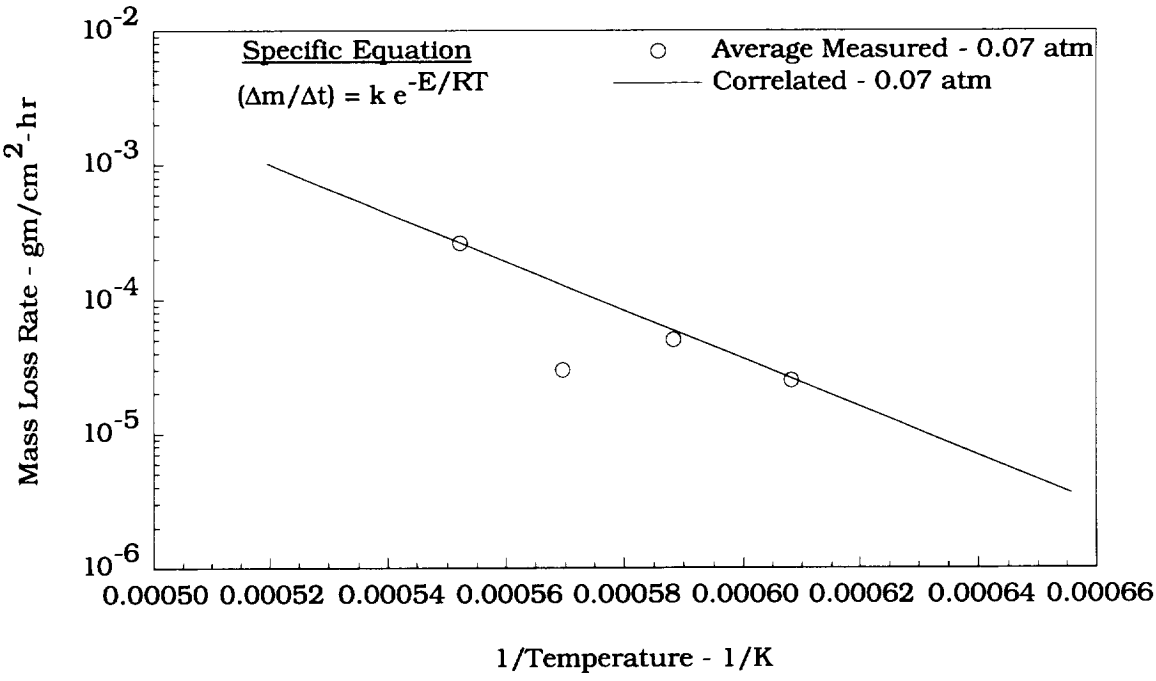

Fig. A-3 Comparison of the Correlated and Average Measured Mass Loss Rate for 0.07-atm DTA Sealant Data.

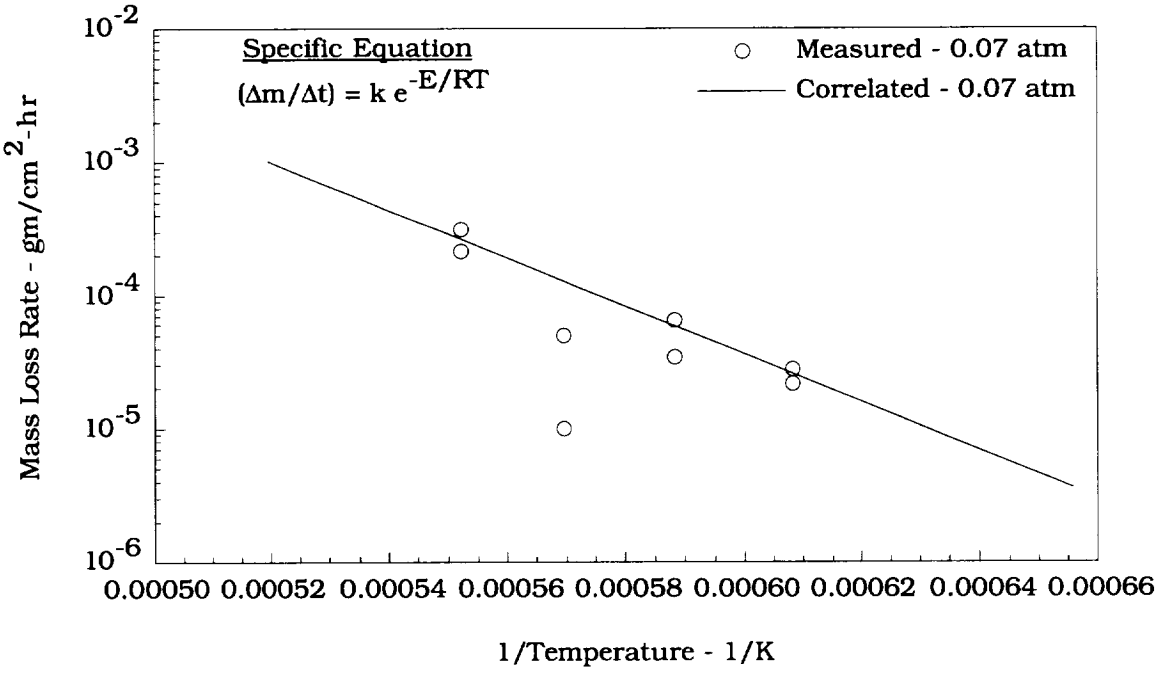

Fig. A-4 Comparison of the Correlated and Measured Mass Loss Rate for 0.07-atm DTA Sealant Data.

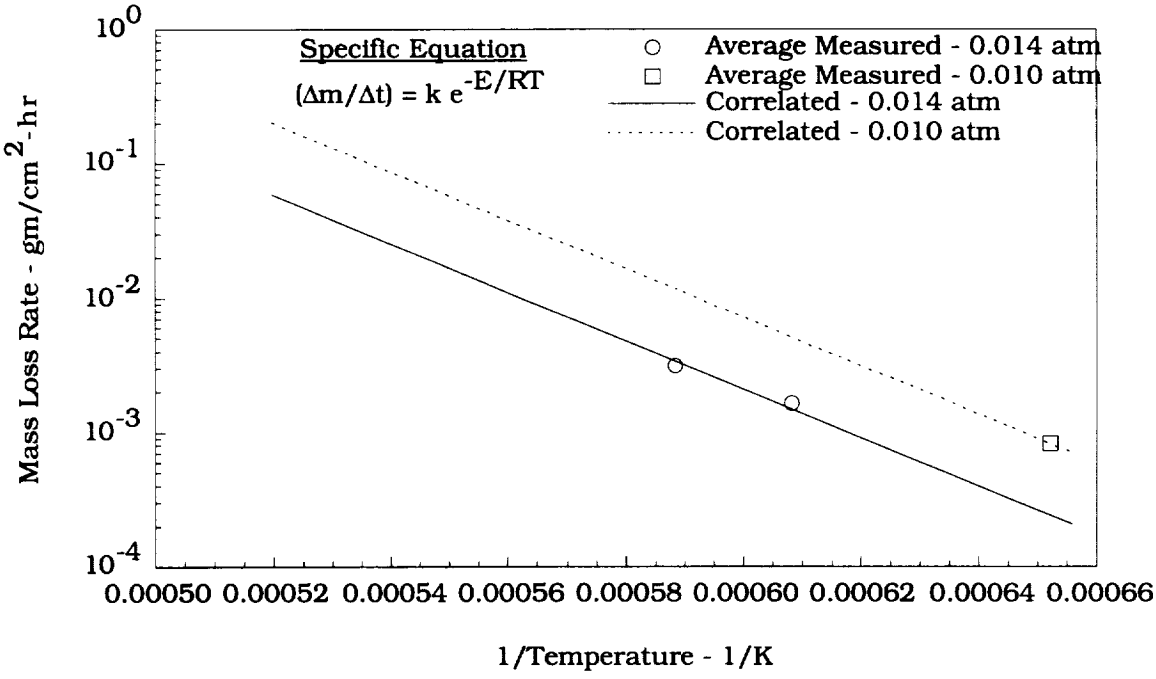

Fig. A-5 Comparison of the Correlated and Average Measured Mass Loss Rate for 0.014-atm and 0.01-atm DTA Sealant Data.

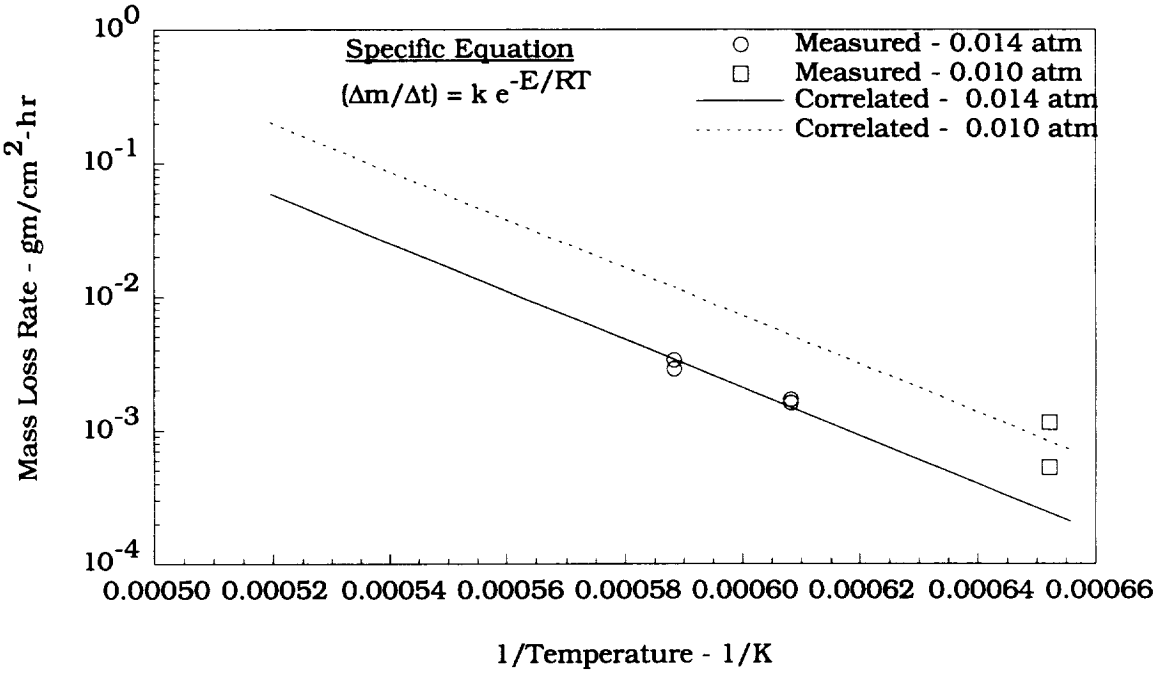

Fig. A-6 Comparison of the Correlated and Measured Mass Loss Rate for 0.014-atm and 0.01-atm DTA Sealant Data.

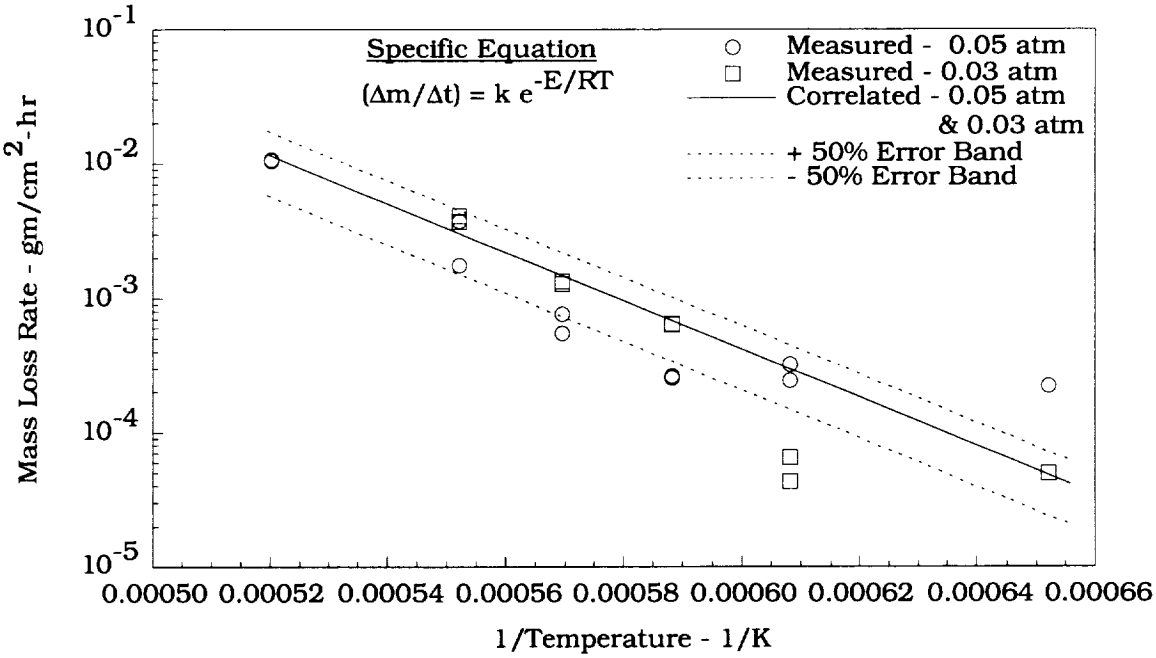

Fig. A-7 Comparison of the Correlated and Measured Mass Loss Rate for 0.05-atm and 0.03-atm DTA Sealant Data With ±50% Error Bands.

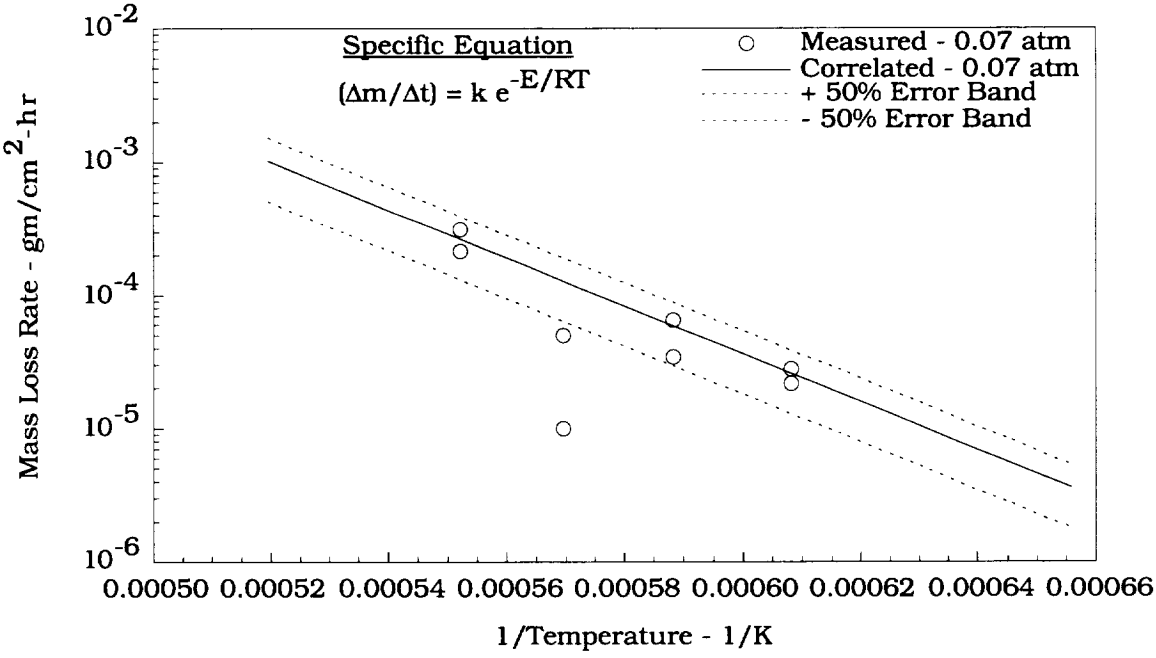

Fig. A-8 Comparison of the Correlated and Measured Mass Loss Rate for 0.07-atm DTA Sealant Data With ±50% Error Bands.

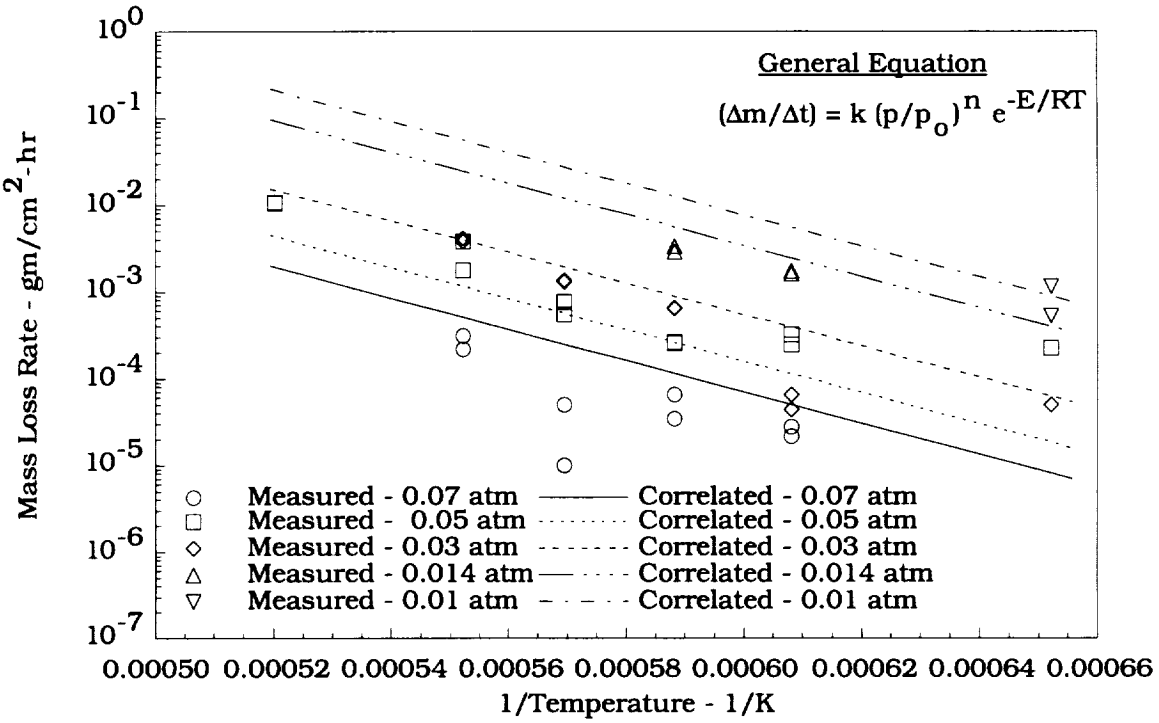

Fig. A-9 Comparison of the Correlated and Measured Mass Loss Rate DTA Sealant Data.

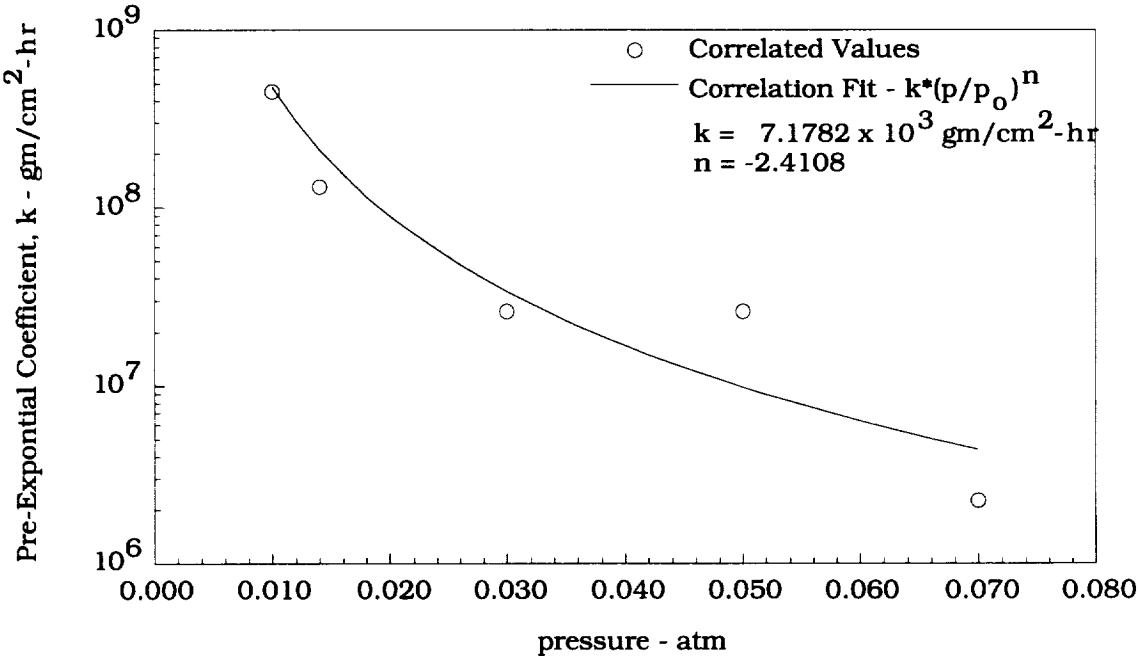

Fig. A-10 Predictions for the Coefficients k and n in the General DTA Equation.

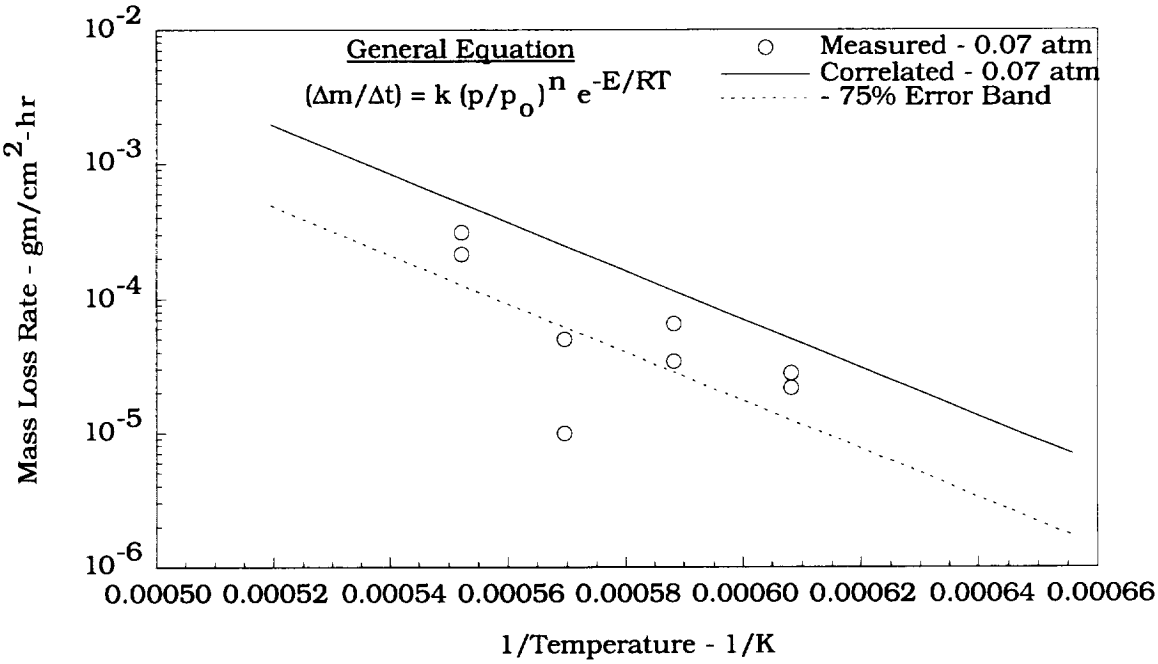

Fig. A-11 Comparison of the General Equation and a -75% Error Band to the 0.07 -atm Measured Mass Loss Rate Sealant Data.

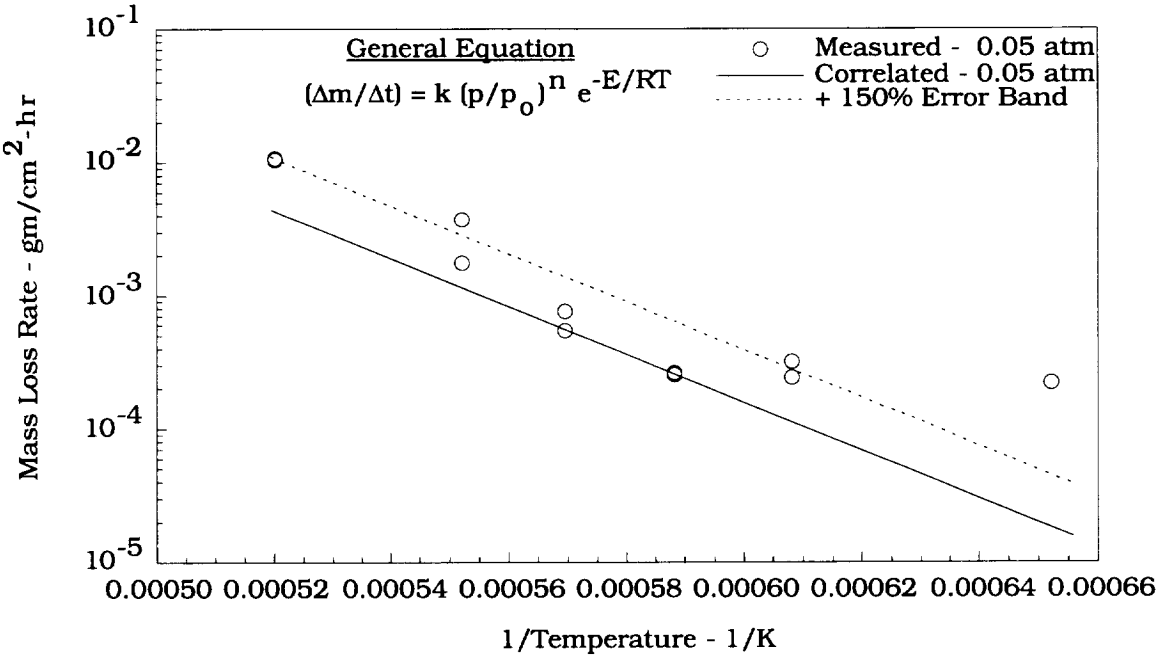

Fig. A-12 Comparison of the General Equation and a +150% Error Band to the 0.05-atm Measured Mass Loss Rate Sealant Data.

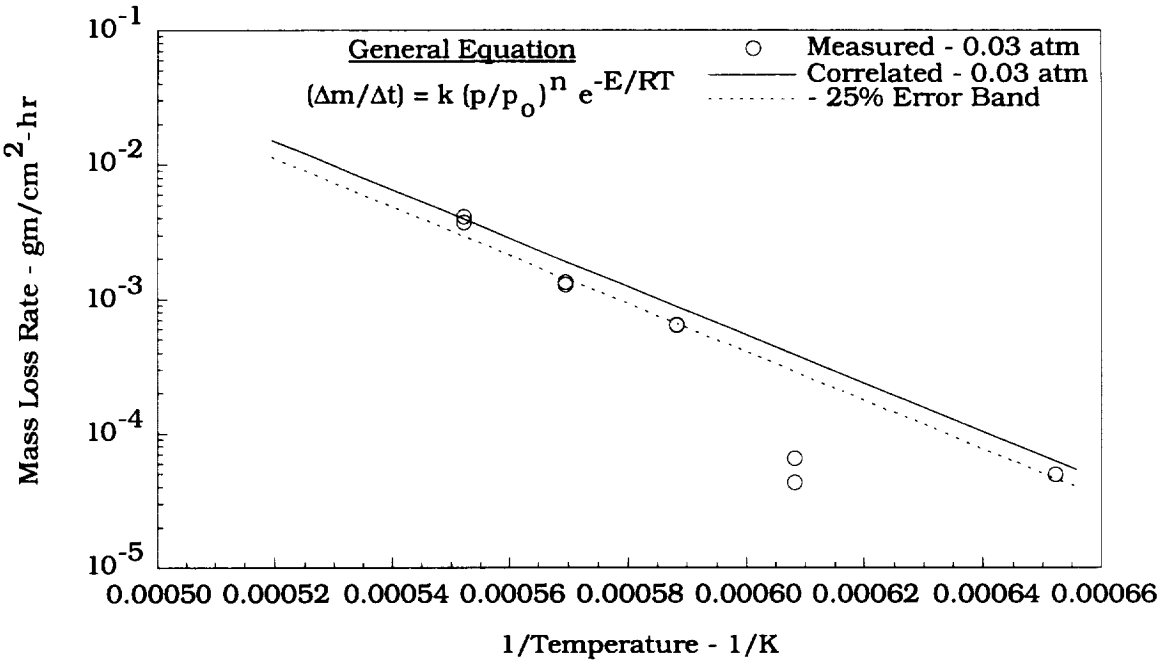

Fig. A-13 Comparison of the General Equation and a -25% Error Band to the 0.03-atm Measured Mass Loss Rate Sealant Data.

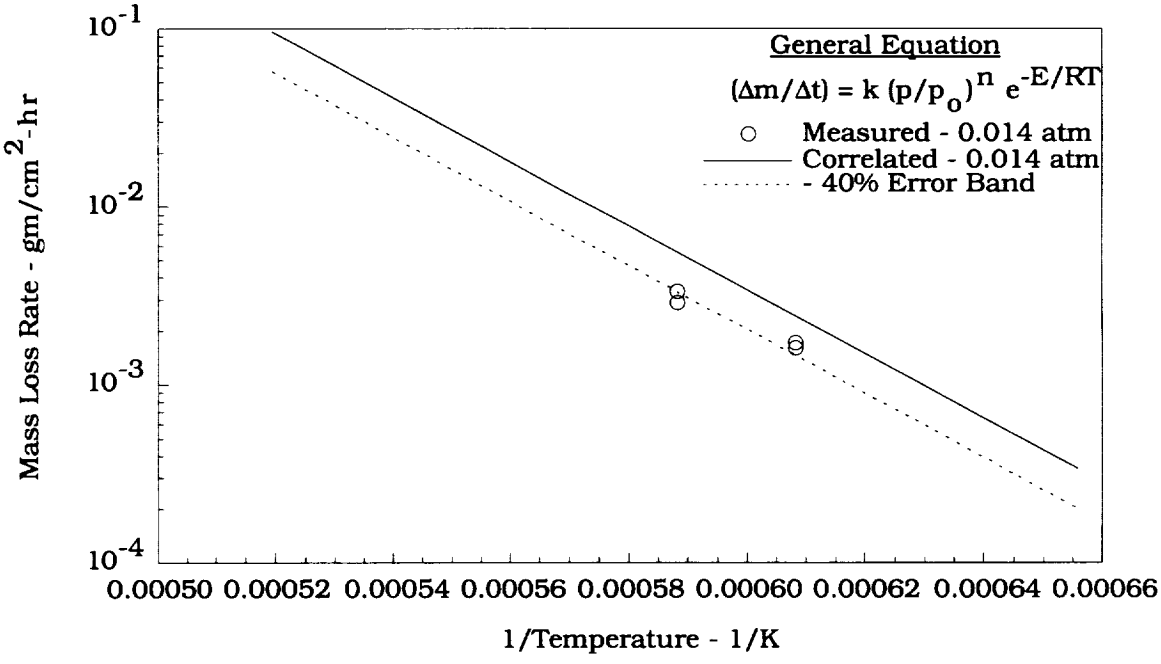

Fig. A-14 Comparison of the General Equation and a -40% Error Band to the 0.014-atm Measured Mass Loss Rate Sealant Data.

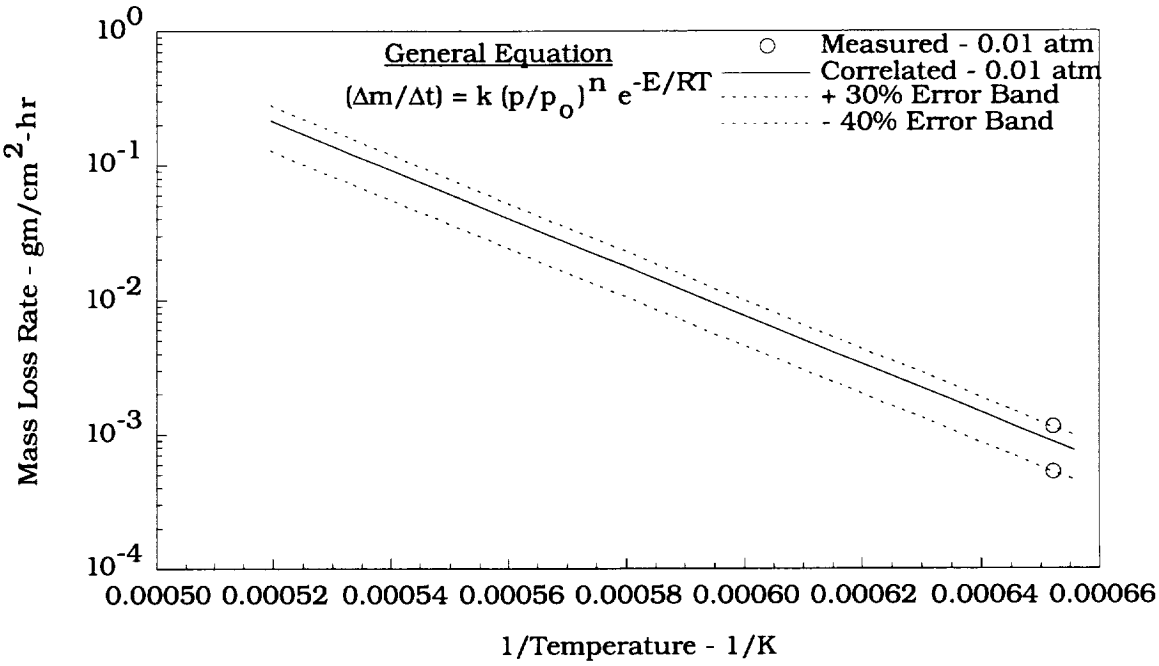

Fig. A-15 Comparison of the General Equation and +30%/-40% Error Bands to the 0.01-atm Measured Mass Loss Rate Sealant Data.

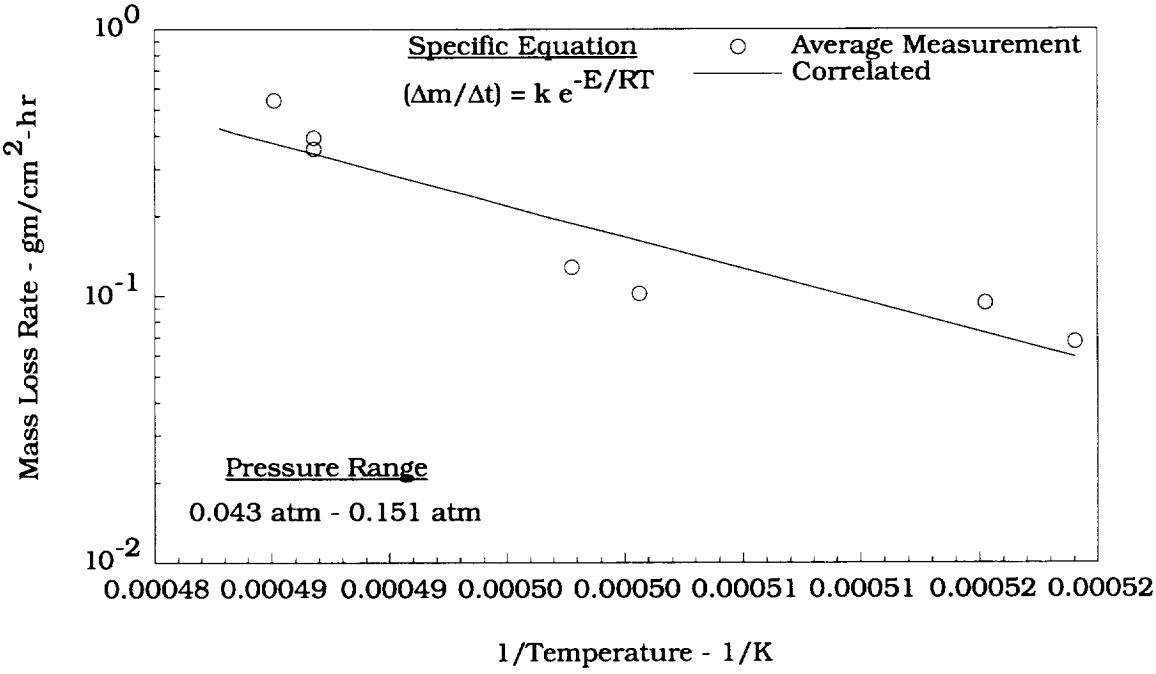

Fig. A-16 Comparison of the Correlated and Average Measured Mass Loss Rate for Over-Temperature Sealant Data.

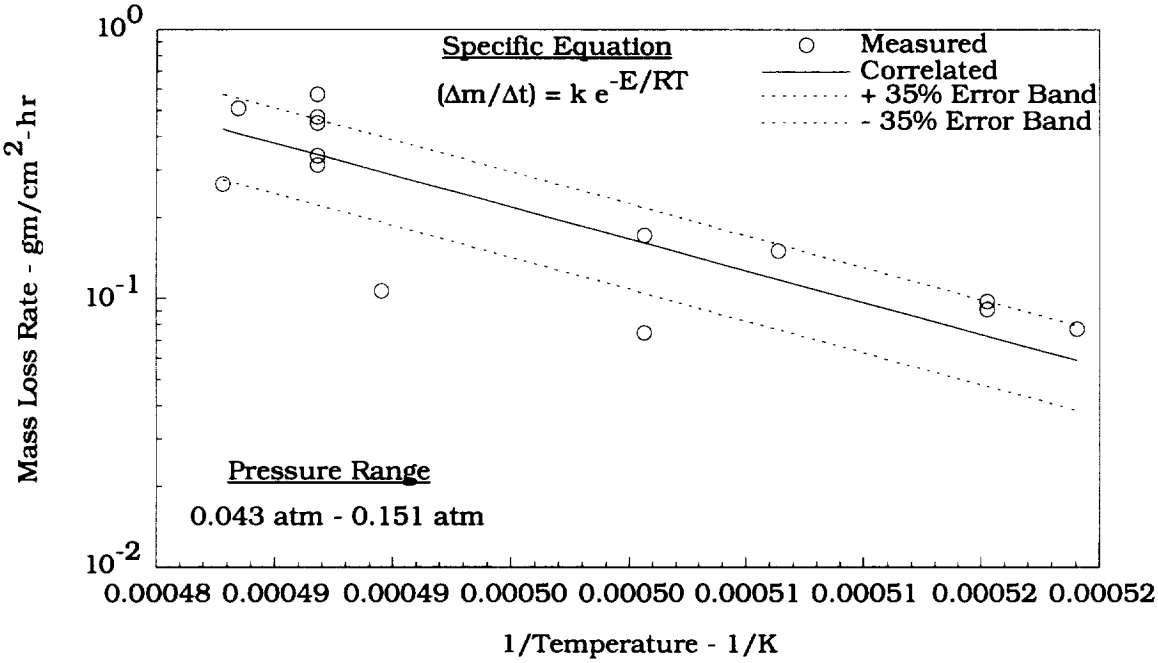

Fig. A-17 Comparison of the Correlated Fit and ±35% Error Bands to the Over-Temperature Measured Mass Loss Rate Sealant Data.

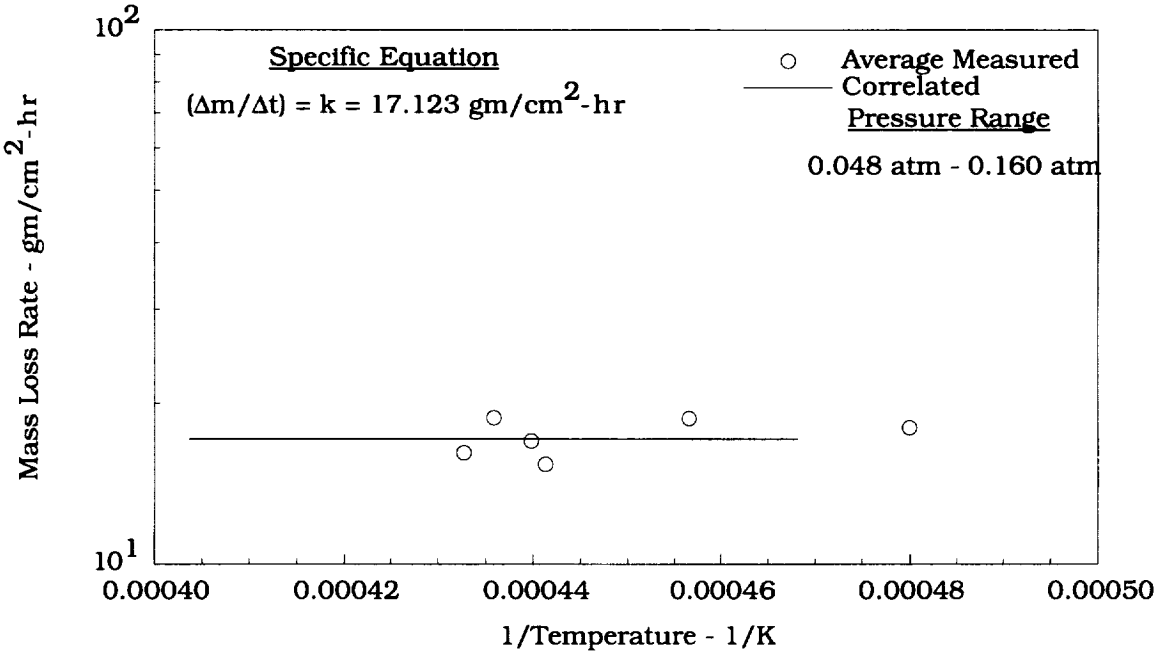

Fig. A-18 Comparison of the Correlated and Average Measured Mass Loss Rate for SiC Coating Diffusion-Limited Data.

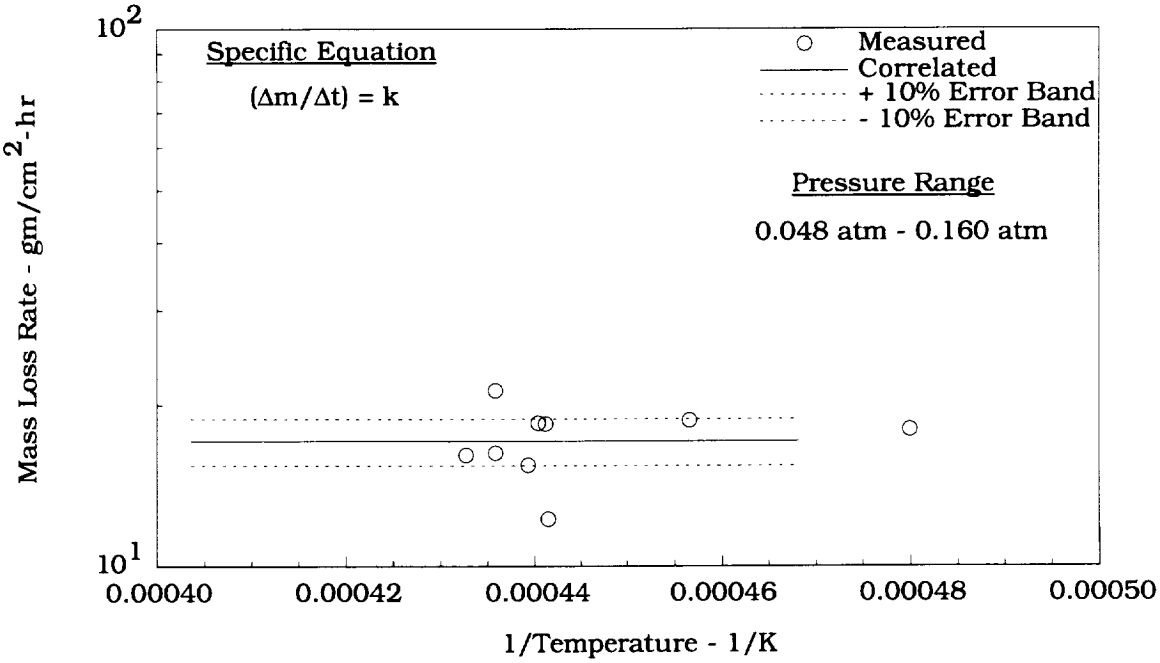

Fig. A-19 Comparison of the SiC Coating Diffusion-Limited Correlation with ±10% Error Bands to the Measured Data.

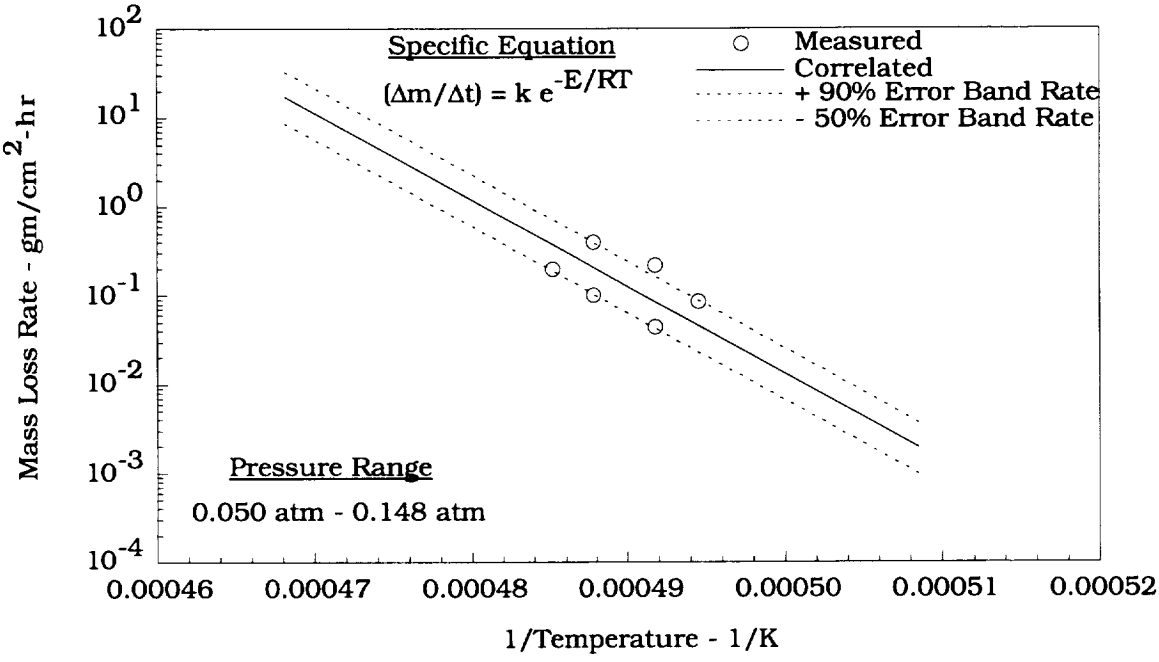

Fig A-20 Comparison of the SiC Coating Rate-Controlled Correlation with +90%/-50% Error Bands to the Measured Data.

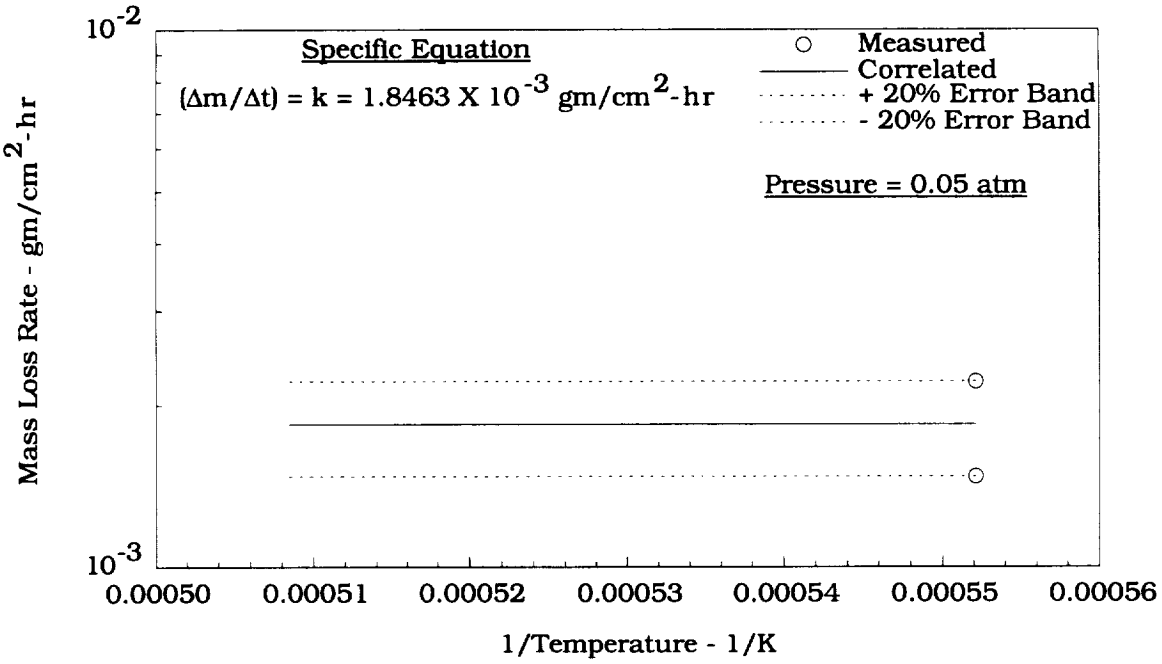

Fig. A-21 Comparison of the SiC Coating Low-Temperature Correlation With ±20% Error Bands to the Measured Data.

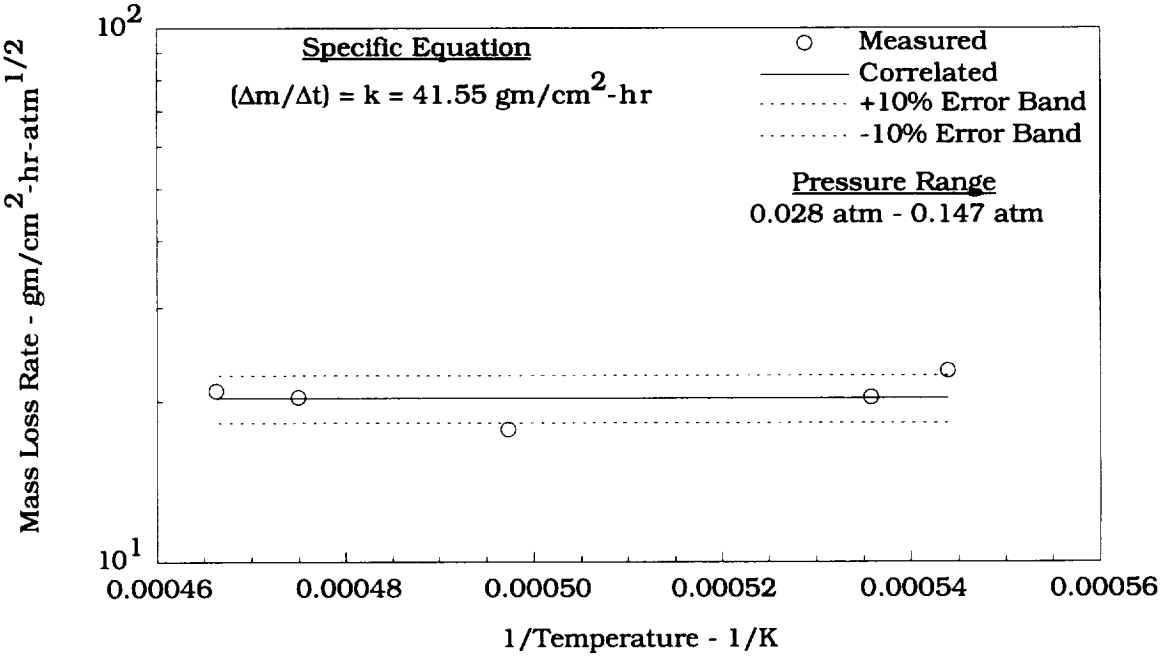

Fig. A-22 Comparison of the RCC Carbon Substrate Diffusion-Limited Correlation With ±10% Error Bands to the Measured Data.

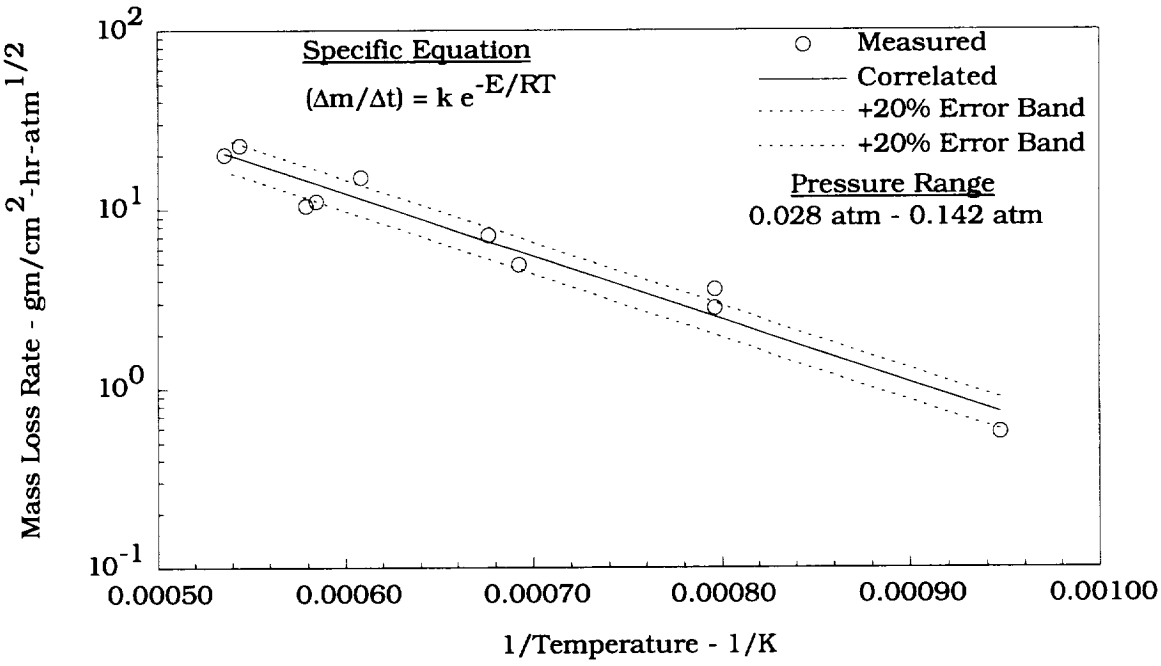

Fig. A-23 Comparison of the RCC Carbon Substrate Rate-Controlled Correlation With ±20% Error Bands to the Measured Data.

Appendix B

RCC Math Model

Appendix B - RCC Thermal Math Model for Arc-Jet Test Simulation

Objectives:
- Assist test design and development
- Support test facility buildup
- Perform pre-test predictions
- Perform post-test thermal analyses and test data correlations

Modeling Assumptions:
- No temperature gradient along the test specimen disk surface
- No thermal contact resistance between the thermocouple insulator sleeve and RCC material
- RCC and graphite holder materials have the same emittance values
- Heat transfer between the thermocouple wires and insulator sleeve is by radiation only
- No thermal contact resistance between the thermocouple bead and the back side of the RCC coating
- Test chamber wall, support arm, and copper cold plate stay at a constant temperature

Model Description:
This thermal math model included the test specimen disk, thermocouple imbedded in the specimen, zirconia insulation disk, model (specimen) holder, copper cold plate, and test environments simulation. The thermal math model was developed for SINDA,[1] and run on the Cray-YMP.

Assuming no temperature gradient across the test specimen surface, the math model represents a 2.54-cm-diameter cut from the top center surface of the test specimen down to the bottom of the copper cold plate. The chamber wall, cold plate, and water-cooled support arm were simulated by three different heat sink nodes. The RCC disk was broken down into seven nodes in depth, with two nodes for each side of the coating, two nodes for bare RCC, and one node for Type A sealant at the top surface. The rest of the nodes were for zirconia insulation, graphite holder, copper cold plate, copper mounting screw, thermocouple wire, insulation sleeve, support arm, and chamber wall. A total of 45 nodes were used. A sketch of the test model, as well as the thermal math model, is shown in figure B-1.

Test environments simulation included surface heating and pressure. For pre-test analysis, the test environments were based on the predetermined pressure and corresponding heating rate for the predetermined temperature. For post-test analysis, the test environments were based on the actual test pressure and calculated non-equilibrium heating rate using the BLIMP program[2] with test enthalpy and pressure.

Material thermal properties used in the math model included the surface emissivity, thermal conductivity, specific heat, and material density. The properties for the RCC sealant, SiC coating and carbon substrate are listed in table B-1. The properties used for the graphite holder are provided in table B-2, while the properties for both the Zirconia board and felt are given in table B-3. The values used for the copper screw and cold plate are provided in table B-4, while the properties used for the thermocouple wire and sleeve are shown in tables B-5 and B-6.

---

[1]Cullimore, B. A.; Goble, R. G; Jensen, C. L.; and Ring, S. G.: User's Manual SINDA/FLUINT Systems Improved Numerical Differencing Analyzer and Fluid Integrator, Ver. 2.6, MCR-91-1393, Martin Marietta Astronautics Group, Denver, CO, Sept. 1993.

[2]Murray, A. L.: Further Enhancements of the BLIMP Computer Code and User's Guide, AFWAL-TR-88-3010, June 30, 1988.

Table B 1 RCC Thermal Properties

Type A Sealant

Density[3] 1.730 gm/cm^3

Conductivity Not known

Specific Heat[4]

Temperature K	Specific Heat cal/gm-K
200	0.09
256	0.15
368	0.20
480	0.23
592	0.24
704	0.26
816	0.27
928	0.27
1040	0.28
1152	0.29
1264	0.30
1376	0.30
1488	0.31
1600	0.32
1712	0.32
1824	0.33
1936	0.34
2048	0.34
2160	0.35

[3]Personal Communication to D. M. Curry from Neal Webster, Loral Corp., 1993.

[4]Pankratz, L. B.: Thermodynamic Properties of Elements and Oxides, Bureau of Mines, Bulletin 672, Jan. 1983.

Table B 1 RCC Thermal Properties (continued)

Silicon Carbide Coating

Density[3] 2.114 gm/cm^3

Specific Heat[4]

Temperature K	Specific Heat cal/gm-K
200	0.05
256	0.13
368	0.19
480	0.23
592	0.25
704	0.26
816	0.27
928	0.28
1040	0.29
1152	0.30
1264	0.31
1376	0.32
1488	0.33
1600	0.34
1712	0.35
1824	0.36
1936	0.37
2048	0.37
2160	0.38

Conductivity[5] 64.07441 cal/cm-sec-K

[3]Personal Communication to D. M. Curry from Neal Webster, Loral Corp., 1993.

[4]Pankratz, L. B.: Thermodynamic Properties of Elements and Oxides, Bureau of Mines, Bulletin 672, Jan. 1983.

[5]Undocumented calculations by D. Chao based on data transmitted with specimens prior to testing, 1988 - 1989.

Table B 1 RCC Thermal Properties (continued)

Carbon Substrate

Density[3] 1.362 gm/cm^3

Carbon-Carbon Specific Heat and Conductivity[6]

Temperature K	Specific Heat cal/gm-K	Temperature K	Conductivity Normal cal/cm-sec-K	Conductivity Parallel cal/cm-sec-K
144	0.12	33	0.01654	0.02579
256	0.17	311	0.12815	0.19991
367	0.21	478	0.17155	0.26762
478	0.24	644	0.19553	0.30631
533	0.26	867	0.21206	0.33211
811	0.31	1144	0.21950	0.34244
1089	0.34	1422	0.22141	0.34501
1367	0.37	1867	0.21702	0.33856
1644	0.40	2200	0.21496	0.33525
1922	0.42			

Surface Emissivity[7]

Temperature K	ε
89	0.385
144	0.600
200	0.760
256	0.781
367	0.800
478	0.821
533	0.831
756	0.864
811	0.872
1033	0.896
1089	0.900
1200	0.900
1311	0.900
1333	0.900
1367	0.890
1422	0.880
1478	0.867
1589	0.833
1644	0.815
1756	0.770
1811	0.745
1922	0.695
2089	0.610

[3]Personal Communication to D. M. Curry from Neal Webster, Loral Corp., 1993.

[6]Personal Communication on new RCC thermal properties to D. Chao from Neal Webster, LTV Corp., Jan. 20, 1987.

[7]Undocumented combination of RCC emissivity values by D. Chao, 1988.

Table B 2 ATJ Graphite Thermal Properties[8]

Density 1.740 gm/cm^3

Temperature K	Specific Heat cal/gm-K	Conductivity cal/cm-sec-K
256	0.140	0.00058
533	0.310	0.00128
811	0.390	0.00161
1089	0.430	0.00178
1367	0.455	0.00188
1644	0.475	0.00196
1922	0.485	0.00200

Use RCC emissivity values.

[8]Personal Communication on thermal properties for graphite holder to D. Chao from Neal Webster, LTV Corp, 1993.

Table B 3 Zirconia Insulation Properties
Zirconia Board - Type ZYFB3 (4-6 micron fibers)[9]

Density 0.481 gm/cm^3

Temperature K	Specific Heat cal/gm-K	Temperature K	Conductivity cal/cm-sec-K
367	0.180	811	0.000207
2644	0.256	1089	0.000277
		1367	0.000343
		1644	0.000446
		1922	0.000587

Emissivity

Temperature K	ε
1283	0.300
1811	0.180

Zirconia Board - Type ZYF100 (4-6 micron fibers)[10]

Density 0.240 gm/cm^3

Temperature K	Specific Heat cal/gm-K	Temperature K	Conductivity cal/cm-sec-K
367	0.130	394	0.000174
2644	0.180	533	0.000207
		811	0.000285
		1089	0.000376
		1367	0.000488
		1644	0.000620
		1922	0.000773

Emissivity

Temperature K	ε
1283	0.300
1811	0.180

[9]Technical Data, Zirconia Insulation Type ZYFB, Bulletin No. ZPI-203, Zicrcar Products, Inc., Flordia, N.Y., June 1992.
[10]Technical Data, Zirconia Felt Type ZYF, Bulletin No. ZPI-207, Zicrcar Products, Inc., Flordia, N.Y., October 1992.

Table B 4 Copper Properties

Density 8.954 gm/cm^3
Specific Heat 0.0915 cal/gm-K

Tempertature K	Conductivity cal/cm-sec-K
173	0.97144
273	0.92184
293	0.92184
373	0.90530
473	0.89290
673	0.86810
873	0.84329

Table B 5 Tungsten with 15% Rhenium Properties[11]

Density 19.603 gm/cm^3
Specific Heat 0.0345 cal/gm-K

Temperature K	ε	Temperature K	Conductivity cal/cm-sec-K
298	0.02	273	0.39684
373	0.03	293	0.38858
811	0.08	373	0.35964
3589	0.39	473	0.33897
		573	0.31830
		673	0.30177
		873	0.26870
		1073	0.26456

Table B 6 Alumina Insulating Cylinder - Type ALC - Properties[12]

Density 0.240 gm/cm^3
Specific Heat 0.25 cal/gm-K

Temperature K	ε	Temperature K	Conductivity cal/cm^2-sec-K
1283	0.30	533	0.000124
1811	0.18	811	0.000207
		1089	0.000310
		1367	0.000446
		1644	0.000620

[11]Calculations by D. Chao combining Tungsten & Rhenium for the math model.

[12]Technical Data, Alumina Insulating Cylinders Type ALC, Bulletin No. ZPI-301, Zicrcar Products, Inc., Flordia, N.Y., August 1992.

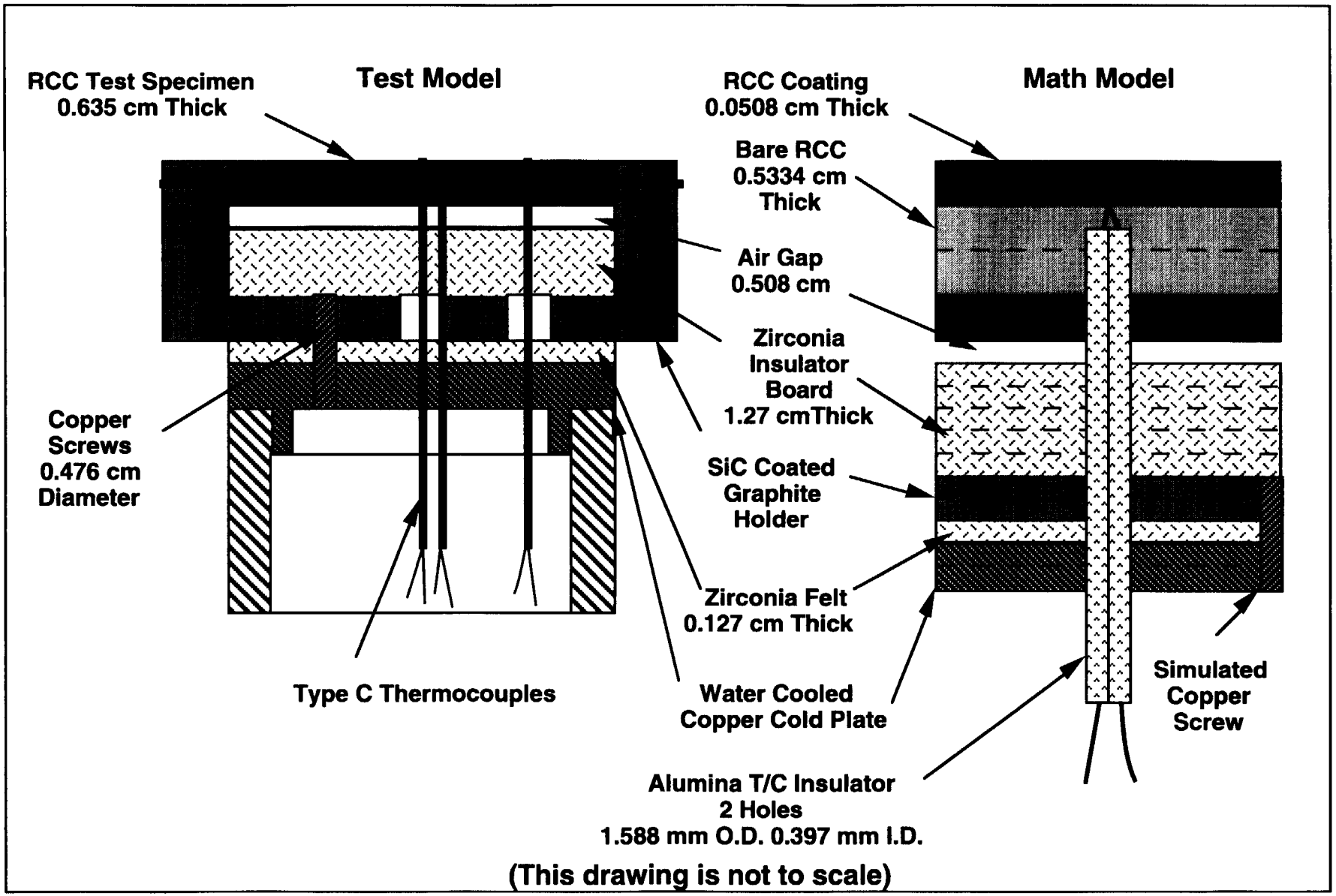

Fig. B-1 Sketch of the RCC Test Model and Simulated Thermal Math Model.

REPORT DOCUMENTATION PAGE

Form Approved
OMB No. 0704-0188

1. AGENCY USE ONLY (Leave Blank)	2. REPORT DATE	3. REPORT TYPE AND DATES COVERED
	Jun/94	Technical Memorandum

4. TITLE AND SUBTITLE
Analysis of the Shuttle Orbiter Reinforced Carbon-Carbon Oxidation Protection System

5. FUNDING NUMBERS

6. AUTHOR(S)
D. M. Curry, S. D. Williams*, Dennis Chao**, and Vuong Pham

7. PERFORMING ORGANIZATION NAME(S) AND ADDRESS(ES)
Lyndon B. Johnson Space Center
Structures and Mechanics Division
Houston, Texas 77058

8. PERFORMING ORGANIZATION REPORT NUMBERS
S-763

9. SPONSORING/MONITORING AGENCY NAME(S) AND ADDRESS(ES)
National Aeronautics and Space Administration
Washington, D.C. 20546-0001

10. SPONSORING/MONITORING AGENCY REPORT NUMBER
TM-104792

11. SUPPLEMENTARY NOTES
* Lockheed Engineering Sciences Company, ** Rockwell International

12a. DISTRIBUTION/AVAILABILITY STATEMENT
unclassified/unlimited
Available from the NASA Center for AeroSpace Information
800 Elkridge Landing Road
Linthicum Heights, MD 21090
(301) 621-0390
Subject category: 34

12b. DISTRIBUTION CODE

13. ABSTRACT *(Maximum 200 words)*
Reusable, oxidation-protected reinforced carbon-carbon (RCC) has been successfully flown on all Shuttle Orbiter flights. Thermal testing of the silicon carbide-coated RCC to determine its oxidation characteristics has been performed in convective (plasma Arc-Jet) heating facilities. Surface sealant mass loss was characterized as a function of temperature and pressure. High-temperature testing was performed to develop coating recession correlations for predicting performance at the over-temperature flight conditions associated with abort trajectories. Methods for using these test data to establish multi-mission re-use (i.e., mission life) and single mission limits are presented.

14. SUBJECT TERMS
carbon-carbon composites, carbon fibers, reinforcing materials, ablation, abort trajectories, temperature effects, erosion, silicon carbides, silicon dioxides, oxidation

15. NUMBER OF PAGES
70

16. PRICE CODE

17. SECURITY CLASSIFICATION OF REPORT	18. SECURITY CLASSIFICATION OF THIS PAGE	19. SECURITY CLASSIFICATION OF ABSTRACT	20. LIMITATION OF ABSTRACT
unclassified	unclassified	unclassified	UL

NSN 7540-01-280-5500

Standard Form 298 (Rev 2-89)
Prescribed by ANSI Std. 239-18
298-102